JBC RESEARCH ARTICLE

The oxidoreductase CLIC4 is required to maintain mitochondrial function and resistance to exogenous oxidants in breast cancer cells

Received for publication, January 19, 2022, and in revised form, June 1, 2022 Published, Papers in Press, July 19, 2022,
https://doi.org/10.1016/j.jbc.2022.102275

Heba Al Khamici[1], Vanesa C. Sanchez[2], Hualong Yan[1], Christophe Cataisson[1], Aleksandra M. Michalowski[1], Howard H. Yang[1], Luowei Li[1], Maxwell P. Lee[1], Jing Huang[1], and Stuart H. Yuspa[1,*]

From the [1]Laboratory of Cancer Biology and Genetics, Center for Cancer Research, National Cancer Center, National Institutes of Health. Bethesda, Maryland, USA; [2]Office of Science, Division of Nonclinical Science, Center for Tobacco Products, U.S. Food and Drug Administration, Silver Spring, Maryland, USA

Edited by Donita Brady

The chloride intracellular channel-4 (CLIC4) is one of the six highly conserved proteins in the CLIC family that share high structural homology with GST-omega in the GST superfamily. While CLIC4 is a multifunctional protein that resides in multiple cellular compartments, the discovery of its enzymatic glutaredoxin-like activity *in vitro* suggested that it could function as an antioxidant. Here, we found that deleting CLIC4 from murine 6DT1 breast tumor cells using CRISPR enhanced the accumulation of reactive oxygen species (ROS) and sensitized cells to apoptosis in response to H_2O_2 as a ROS-inducing agent. In intact cells, H_2O_2 increased the expression of both CLIC4 mRNA and protein. In addition, increased superoxide production in 6DT1 cells lacking CLIC4 was associated with mitochondrial hyperactivity including increased mitochondrial membrane potential and mitochondrial organelle enlargement. In the absence of CLIC4, however, H_2O_2-induced apoptosis was associated with low expression and degradation of the anti-apoptotic mitochondrial protein Bcl2 and the negative regulator of mitochondrial ROS, UCP2. Furthermore, transcriptomic profiling of H_2O_2-treated control and CLIC4-null cells revealed upregulation of genes associated with ROS-induced apoptosis and downregulation of genes that sustain mitochondrial functions. Accordingly, tumors that formed from transplantation of CLIC4-deficient 6DT1 cells were highly necrotic. These results highlight a critical role for CLIC4 in maintaining redox-homeostasis and mitochondrial functions in 6DT1 cells. Our findings also raise the possibility of targeting CLIC4 to increase cancer cell sensitivity to chemotherapeutic drugs that are based on elevating ROS in cancer cells.

Reactive oxygen species (ROS) can be produced through enzymatic reactions by NADPH oxidases, lipoxygenase, cytochrome P450, and cyclooxygenase (1). Nonenzymatic reactions such as those resulting from the mitochondrial respiratory chain also contribute to the production of ROS in cells (1). In cancer cells, elevated ROS may result as a consequence of oncogene activation during the transformation of cells (2–4), dysfunctional mitochondria, increased activity of oxidases, and increased cellular receptor signaling or through crosstalk with infiltrating immune cells (5). ROS-sensitive signaling pathways that are involved in cell proliferation and differentiation, regulating protein synthesis, glucose metabolism and cell survival and inflammation are persistently elevated in many cancer types (6–8). Furthermore, low endogenous concentrations of hydrogen peroxide and superoxides stimulate cell proliferation in a variety of cancer types (5, 9).

In contrast, antioxidants to block oxidative stress are reported to reverse the cancer phenotype in some cases (10–12). Increasing the expression of catalase and glutathione peroxidases reduced cancer cell proliferation and cell doubling (13, 14). In fact, an early approach to treat cancer used antioxidant agents to target ROS (15, 16). However, obtaining consistent results was challenging and, in some cases, using antioxidants promoted cancer initiation and progression leading to the use of ROS inducers as anticancer agents in order to overcome the specific threshold of ROS level beyond which cancer cells undergo ROS-mediated cell death (17, 18).

While much attention has been directed to catalase, superoxide dismutases (SODs) and GSH as intracellular antioxidants, less attention was focused on the antioxidant properties of the chloride intracellular channel-4 (CLIC4). CLIC4 is a member of a highly conserved family of six mammalian proteins that share high structural homology with glutathione-S-transferases (GSTs) and in particular the GST-omega class. CLIC4 is highly abundant in cells and specifically localized to the nucleus, mitochondria, and the endoplasmic reticulum as well as a major cytoplasmic component (19, 20). CLIC4 is highly redox sensitive (21, 22) and metamorphic with the ability to switch between two different structural conformations (21) to carry multiple functions. The cytoplasmic soluble form of CLIC4 exerts a glutaredoxin-like enzymatic function *in vitro* (23), and when membrane bound, it was speculated to function as a poorly selective anion channel (22). CLIC4 is involved in multiple cellular functions including angiogenesis

* For correspondence: Stuart H. Yuspa, yuspas@mail.nih.gov.

(24–26), immune system activity (27–30), epithelial and myofibroblast differentiation (31–34), tumor necrosis factor-α mediated apoptosis (35), transforming growth factor beta signaling (34), and in cancer development and progression where its expression is particularly high in tumor stroma and is linked to the formation of cancer associated fibroblasts (34, 36–41). This multitude of functions and paralogs within species and the high conservation of CLIC homologs across species suggested that the CLIC family of proteins perform a fundamental life purpose.

We postulated that CLIC4 could participate in regulating the oxidative environment in cancer cells. Further, the soluble fraction of CLIC4 might serve as a protective mechanism for cellular and mitochondrial damage generating ROS in response to exogenous toxins such as oxidants or certain anticancer drugs (41–43). It is well known that breast cancer cells have higher ROS than their normal counterparts (44, 45), and the molecular mechanisms involving ROS in the growth, invasiveness, and metastatic spread of breast cancer is not understood. In human breast cancer, the high expression of CLIC4 was associated with poor outcome and enhanced disease progression (46). Herein, we used murine breast cancer cells proficient or deficient in CLIC4 to study the influence of oxidative stress and breast cancer redox homeostasis to shed light on the role of CLIC4 that contributes to the growth and viability of those cancer cells.

Results

CLIC4-null 6DT1 cells have high ROS content

While the oxidoreductase activity of CLIC4 was established with recombinant protein, similar properties have not been confirmed in cells. To address this issue, we used murine breast cancer cell line 6DT1 cells (47) and stable CLIC4-deficient 6DT1 clones (sg# 1 and sg# 2) that were isolated using CRISPR. First, we investigated the localization of CLIC4 in WT 6DT1 cells and found that CLIC4 is widely expressed in cells without treatment and abundant in mitochondria. Adding 500 nM of H_2O_2 to cells increased the expression of CLIC4 in 6DT1 cells (Fig. 1*A*).

The intrinsic ROS was measured using CellROX green or CM-H2DCFDA. Confocal imaging results of whole cell projection showed that untreated CLIC4 KO 6DT1 cells (CLIC4-KO) displayed higher fluorescence for CellROX green than WT cells (Fig. 1*B*), while fluorescent intensity was similar for both genotypes 24 h after treatment with 1 μM of H_2O_2. After incubation with CM-H_2DCFDA, fluorescence-activated cell sorting (FACS) analysis (Fig. 1*C*) confirmed that ROS is elevated in untreated CLIC4-KO cells at baseline level. The mean fluorescence intensity of three independent repeats also showed that treating the 6DT1 cells with H_2O_2 increased the level of ROS in CLIC4-WT but not the CLIC4-KO 6DT1 cells, as quantified in Figure 1*D*. The ROS disparities among the genotypes disappeared when cells were preincubated with the general antioxidant N-acetyl cysteine or NAC (Fig. 1, *C* and *D*).

These results indicated that CLIC4 participated in an intrinsic antioxidant environment in untreated cancer cells, but compensatory pathways were available for protection from an extrinsic oxidative insult.

CLIC4-WT 6DT1 cells have higher tolerance to H_2O_2 than the CLIC4-KO cells

To determine the functional consequences of ROS alterations, WT, KO, and CLIC4 KO reconstituted with CLIC4 6DT1 breast cancer cells were exposed to different concentrations of H_2O_2 and tested for cell viability (CCK-8) and cell proliferation responses (CyQuant).

There was no significant baseline difference in cell viability percentage among cells that do or do not express CLIC4 over 7 days (Fig. 2*A*). However, 6DT1 cells treated with different concentrations of H_2O_2 for 24 h exhibited attenuated cell viability in a dose-dependent manner, while the loss of viability in CLIC4-KO was substantially accelerated as the concentration of H_2O_2 increased when compared to WT and KO cells reconstituted with CLIC4 *via* lentivirus (KO+CLIC4) (Fig. 2*B*). Similar results were observed with a second CLIC4-KO (sg# 2) clone (Fig. S1). As seen in Figure 1, the sensitivity to H_2O_2 is ROS mediated in all genotypes since viability was restored by incubating the cells with catalase or NAC with/without H_2O_2 (as shown in Fig. 2, *C* and *D*). Loss of CLIC4 also sensitized 6DT1 cells to the antiproliferative effects of increasing the concentration of H_2O_2 to 1 μM in comparison to the cells that express CLIC4 (WT and KO+CLIC4) as shown in Figure 2*E*. Post-incubating the cells with catalase (Fig. 2*F*) or NAC (Fig. 2*G*) in the presence or absence of H_2O_2 restored proliferation of CLIC4 null cells to the same levels as the cells that express the protein.

CLIC4 expression is upregulated by H_2O_2 in breast cancer cells

While the loss of CLIC4 leads to a pro-oxidant internal environment, we asked if CLIC4 was elevated in response to an external pro-oxidant environment. In Figure 3, *A* and *B*, increasing concentrations of H_2O_2 induced the expression of CLIC4 protein and transcripts in WT 6DT1 cells as well as in 4T1 breast cancer cells as in Figure 3*C*. The induction of CLIC4 transcripts was in response to a pro-oxidant environment as it was mitigated by cotreatment with NAC (Fig. 3*B*). There was little or no change of catalase, CLIC1, and GST-omega 1 proteins in WT 6DT1 cells. In contrast, in the absence of CLIC4, H_2O_2 elicited an increased induction in SOD1 and SOD2 proteins. Interestingly, while the DNA damage marker yH2Ax was elevated in WT cells under treatment with H_2O_2, it was initially higher in CLIC4-KO cells and remained higher regardless of H_2O_2 treatment. The compensatory increased expression of SOD1 and SOD2 proteins in CLIC4-KO cells suggests an increase in H_2O_2 results from the dismutation of superoxide to H_2O_2 and water.

These results indicated that the CLIC4 response could be an essential protection for oxidative stress or H_2O_2-induced apoptosis in 6DT1 and 4T1 cells.

Loss of CLIC4 increases mitochondrial superoxide and peroxidase activity

While the loss of CLIC4 was associated with elevated intracellular H_2O_2, the source of this elevation was not yet

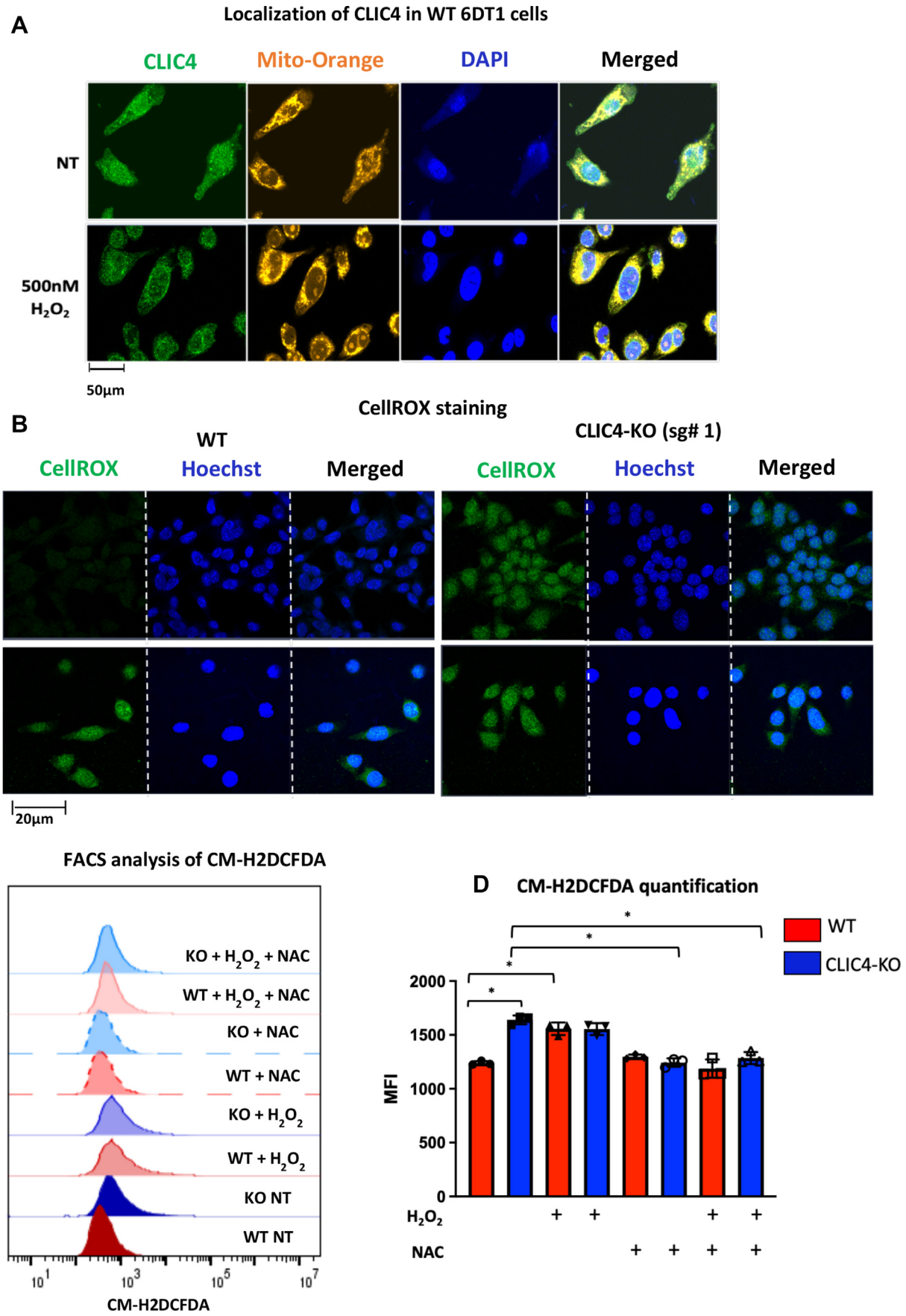
A
Localization of CLIC4 in WT 6DT1 cells
CLIC4
Mito-Orange
DAPI
Merged
NT
500nM H_2O_2
50µm
B
CellROX staining
WT
CLIC4-KO (sg# 1)
CellROX
Hoechst
Merged
CellROX
Hoechst
Merged
NT
1µM H_2O_2
20µm
C
FACS analysis of CM-H2DCFDA
KO + H_2O_2 + NAC
WT + H_2O_2 + NAC
KO + NAC
WT + NAC
KO + H_2O_2
WT + H_2O_2
KO NT
WT NT
Cells Population
10^1
10^3
10^5
10^7
CM-H2DCFDA
D
CM-H2DCFDA quantification
WT
CLIC4-KO
MFI
2000
1500
1000
500
0
H_2O_2
NAC
+
+
+
+
+
+
+
+
*
*
*
*
*

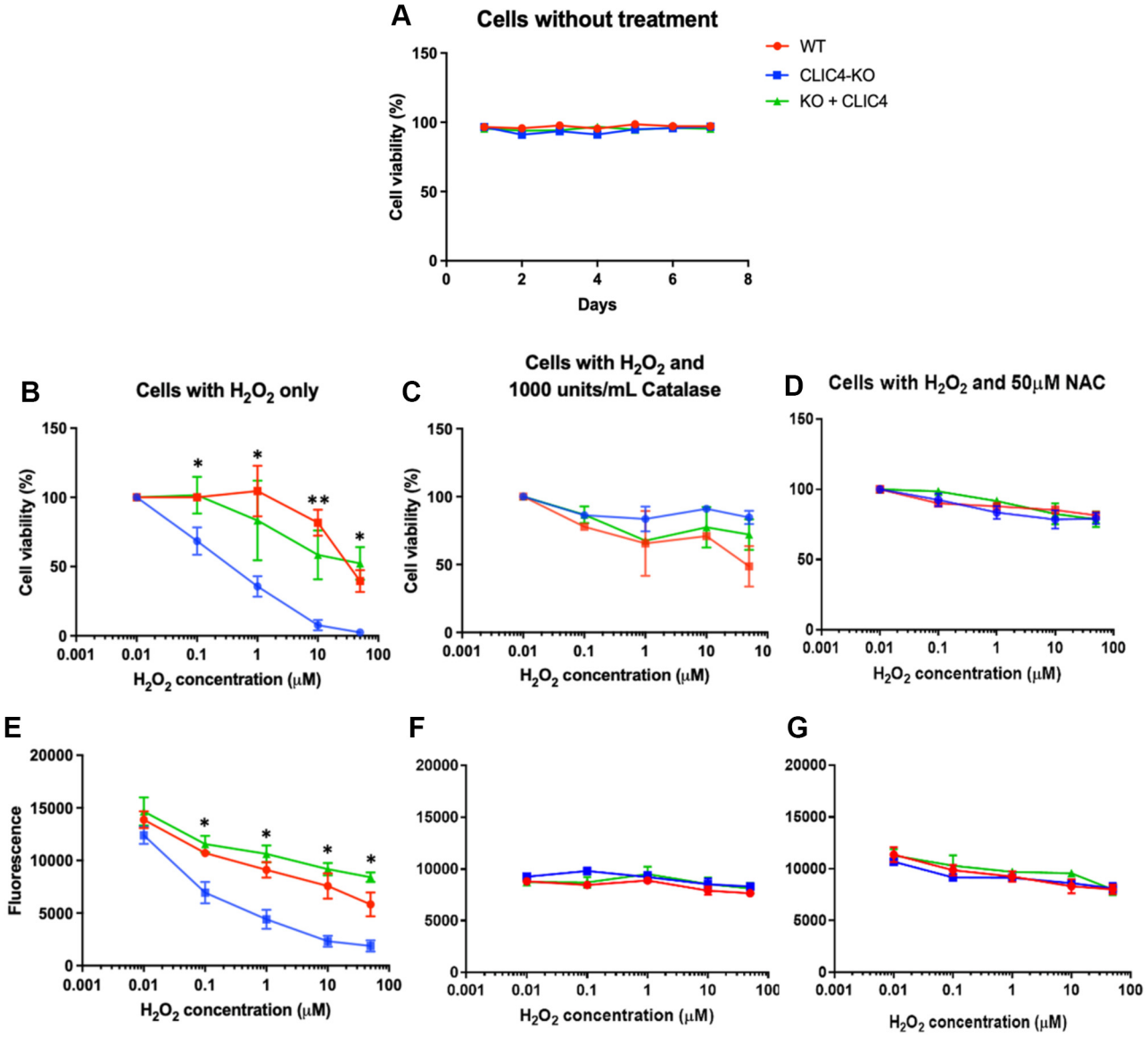

Figure 2. Oxidative stress induced changes in viability and proliferation of 6DT1 cell genotypes. 6DT1 cells were grown in 96-well plates containing phenol red–free Dulbecco's modified Eagle's medium with 10% fetal bovine serum for 24 h at 37 °C and 5% CO_2. *A*, cell viability of CLIC4-WT, KO clone sg# 1, or CLIC4-KO 6DT1 cells transduced with CLIC4 *via* recombinant lentivirus (KO+CLIC4), was determined over 7 days by measuring the absorbance at 450 nm of cells incubated with CCK-8 for 2 h. The absorbance readings were normalized to the nontreated cells of each condition, and numbers were converted to percentage. *B*, viability of CLIC4 WT, CLIC4-KO (clone sg# 1), and KO+CLIC4 6DT1 cells treated with increasing concentrations of H_2O_2 with and without Catalase (*C*) or NAC (*D*) was measured after 24 h. *E*, cell proliferation was assayed 24 h after exposure to increasing concentrations of H_2O_2 or with further addition of Catalase (*F*) or NAC (*G*) by CyQuant fluorescence (480/520 nm). The results were analyzed using prism pad 7 and data were presented as means ± SD of three independent experimental repeats. *$p < 0.05$, **$p < 0.005$. CLIC4, chloride intracellular channel-4; NAC, N-acetyl cysteine.

defined. In cells, ROS is generated as a byproduct of oxidative phosphorylation by the mitochondria or by NADPH oxidases in cell membranes. Mitochondrial superoxides form from one-electron reduction of molecular oxygen (O_2) in complexes I and III (48) and their accumulation in cells is highly associated with oxidative stress and redox signaling and may cause damage to proteins containing iron-sulfur clusters (48).

Previous studies in isolated mitochondria subfractions from rat cardiomyocytes showed that CLIC4 was enriched in the outer mitochondrial membrane fraction with a smaller

Figure 1. General ROS content in 6DT1 cells. *A*, 6DT1 CLIC4-WT cells were either left untreated or treated with 500 nM H_2O_2 for 24 h and incubated with 0.5 μM Mito-tracker orange for Mito-Tracker Orange CMTMRos (*orange*) for 30 min before fixation with 4% paraformaldehyde. Cells were then prepared for staining with CLIC4-specific antibody and Alexafluor-488 (*green*) and DAPI (*blue*) for nuclear staining. Cells were examined with confocal microscopy for immunofluorescence at 63× magnification. *B*, CLIC4-WT and CLIC4 KO (CLIC4-KO clone sg# 1) 6DT1 cells were incubated with 1 μM H_2O_2 for 24 h and stained with 3 μM CellROX green for 30 min and examined by confocal microscopy at 63× optical magnification. *Green* fluorescence is indicative of ROS levels and *blue* is Hoechst nuclear staining. *C*, stacked histogram plot of a representative FACS analysis of WT or KO clone sg# 1 6DT1 cells at 80% confluence that were treated with 1 μM H_2O_2 or 50 μM NAC or both for 24 h followed by addition of 5 μM DCFDA in 1× PBS for 30 min. The shift in cell populations to the *right* under different treatments represents the increase in DCFDA fluorescence. *D*, the mean fluorescence intensity of three independent experiments of 6DT1 cells with indicated treatments, incubated with DCFDA, and evaluated by FACS. The results were plotted using prism pad 7 and data were presented as means ± SD of three independent experimental repeats; *$p < 0.05$. CLIC4, chloride intracellular channel-4; ROS, reactive oxygen species; NAC, N-acetyl cysteine.

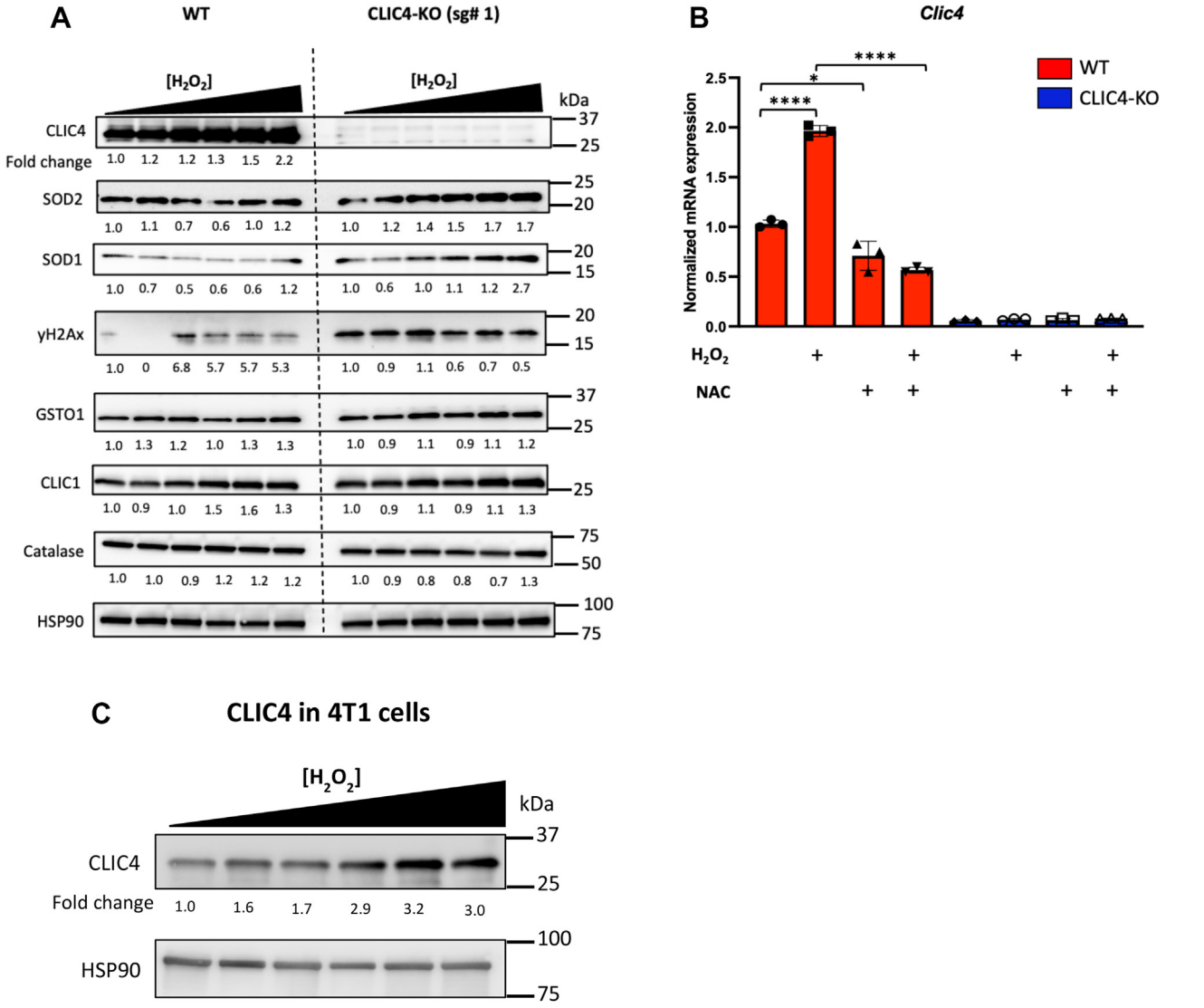

Figure 3. H_2O_2 induces gene and protein expression of CLIC4. *A*, 6DT1 CLIC4-WT or KO clone sg# 1 cells were treated with 0, 0.1 μM, 0.5 μM, 1 μM, 10 μM, and 50 μM of H_2O_2 for 24 h, and lysates were subjected to immunoblotting for expression of intracellular antioxidants and DNA damage (γH2Ax). *B*, CLIC4-WT and KO clone sg# 1 6DT1 cells were treated with 10 μM H_2O_2 and/or 50 μM NAC for 24 h, and the lysates were used for real-time PCR analysis of *Clic4* gene. The results were analyzed using prism pad 7 and data were presented as means ± SD of three independent experimental repeats. *$p < 0.05$, ****$p < 0.0001$. *C*, 4T1 cells were treated with 0, 0.1 μM, 0.5 μM, 1 μM, 10 μM, and 50 μM of H_2O_2 for 24 h, and lysates were subjected to immunoblotting for expression of CLIC4 protein. CLIC4, chloride intracellular channel-4; NAC, N-acetyl cysteine.

subfraction partitioning with the inner mitochondrial membrane (49). In contrast, *in situ* immunogold electron microscopy (EM) of human keratinocytes indicated that CLIC4 localized mainly with the inner mitochondrial membrane and cristae with occasional gold particles in the mitochondrial matrix (50). Thus, both methods suggest that CLIC4 is associated with mitochondrial membranes, but functional studies are required to determine if the protein could participate in the regulation of mitochondrial membrane potential. Confocal microscopy using MitoSOX red (Fig. 4*A*) detected a substantial increase in superoxide generated in CLIC4-null relative to WT 6DT1 cells.

FACS histograms of fluorescence intensity (Fig. 4*B*) and quantification of mean fluorescent intensity (Fig. 4*C*) confirmed the higher level of superoxide in CLIC4-null cells than WT at baseline, and this difference was mitigated by treatment with NAC. WT 6DT1 cells displayed increased intensity when treated with H_2O_2 and the fluorescence intensity decreased upon treatment with 50 μM NAC in both genotypes.

Since the CLIC4-null 6DT1 cells displayed higher superoxide content, we measured the H_2O_2 content in cells. Using Amplite colorimetric hydrogen peroxide assay kit, the total content of H_2O_2 in fresh lysates of CLIC4-KO and WT cells was determined. As shown in Figure 4*D*, the baseline level of H_2O_2 in CLIC4-KO cells and those reconstituted with an empty lentiviral vector was significantly higher than the cells that express CLIC4 (WT) and CLIC4-KO cells reconstituted with CLIC4. Treatment with NAC lowered H_2O_2 levels in all genotypes. Treatment with exogenous H_2O_2 elevated the intracellular H_2O_2 in WT cells to the constitutive levels in CLIC4-null cells. NAC was sufficient to decrease the H_2O_2 levels in all genotypes. Surprisingly, no significant differences

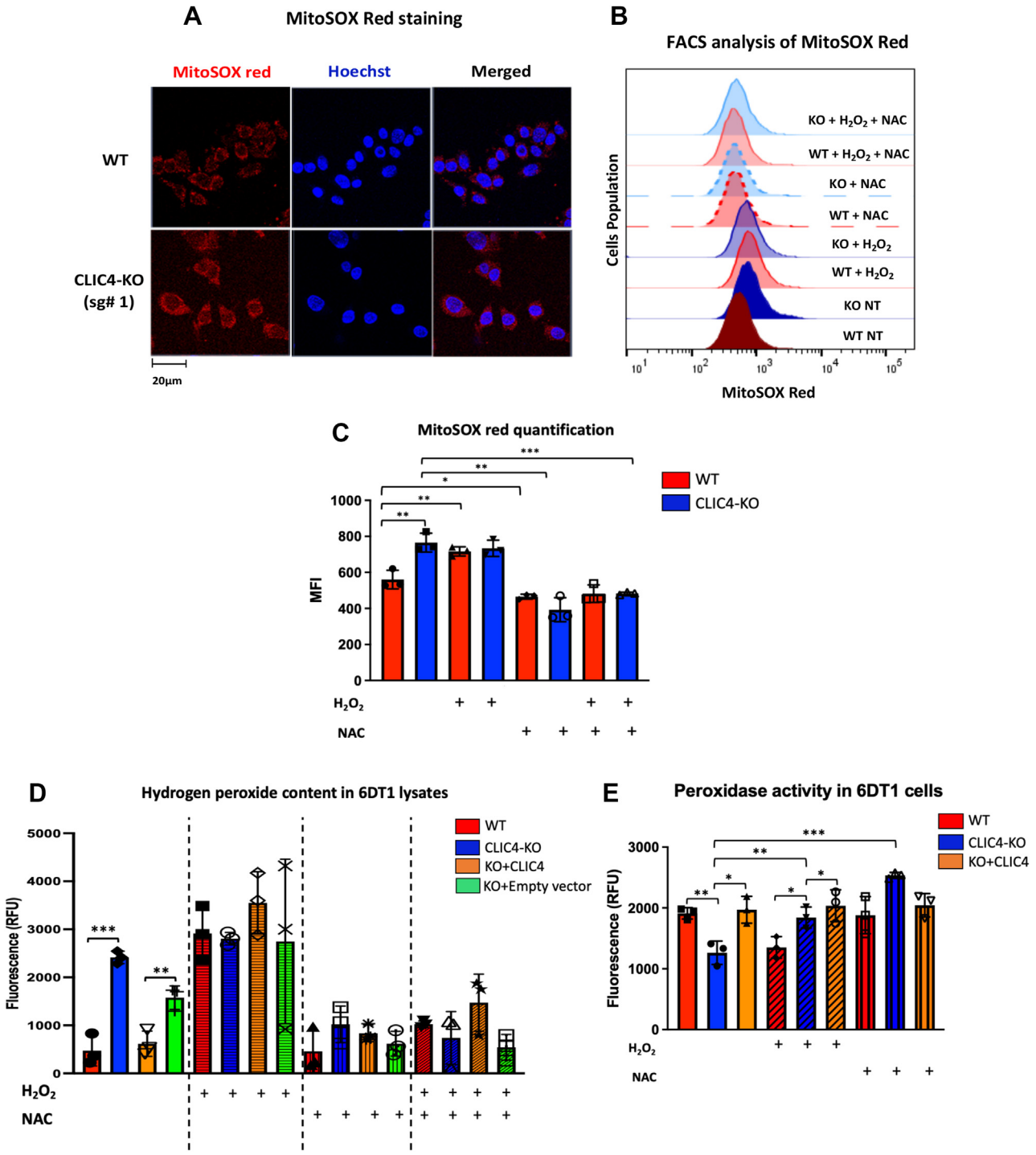

Figure 4. CLIC4-deficient 6DT1 cells have higher mitochondrial superoxides and H_2O_2 content. *A*, CLIC4-WT and KO sg# 1 6DT1 cells were grown to 80% confluence in phenol red–free Dulbecco's modified Eagle's medium incubated with/without 1 μM H_2O_2 for 24 h and exposed to 2 μM MitoSOX red in HBSS for 10 min. *Blue* is Hoechst dye for nuclear staining. Live cell confocal imaging was performed at 63× magnification. *B*, CLIC4-WT and KO clone sg# 1 6DT1 cells were untreated (NT) or treated with 1 μM H_2O_2 or 50 μM NAC or both for 24 h, exposed to 2 μM of MitoSOX red for 10 min, and harvested with trypsin-EDTA and prepared for FACS analysis. The representative stacked histogram plots of FACS analysis indicate the shift in cell populations toward the *right* suggesting higher MitoSOX fluorescence. *C*, averaged mean fluorescence intensity reading plotted from three independent repeats of FACS analysis using MitoSOX red on cells treated as in (*B*) to depict the relative superoxide content by genotype and treatment. *D*, CLIC4-WT, KO clone sg# 1, and KO+CLIC4 lentivirus or control vector (Empty) 6DT1 cells were untreated or incubated with 1 μM H_2O_2 only or 50 μM NAC only or with both (as indicated with the plus + signs under the plot) for 24 h. Amplite substrate was added to fresh cell lysates for 30 min to quantify H_2O_2 content measuring fluorescence at 650 nm. *E*, peroxidase activity was determined in 6DT1 CLIC4-WT cells, CLIC4-KO clone sg# 1, and KO+CLIC4 untreated or treated with 1 μM H_2O_2 with or without 50 μM NAC for 24 h. The red-fluorescent oxidation product, resorufin, indicative of peroxidase activity in 6DT1 cell lysates was measured at 530 to 560/590 nm. *$p < 0.05$, **$p < 0.005$ and ***$p < 0.0005$. CLIC4, chloride intracellular channel-4; NAC, N-acetyl cysteine.

were detected in catalase activity in fresh cell lysates among all cell types (Fig. S2*A*).

As shown in Figure 4*E*, CLIC4-deficient cells had lower peroxidase activity than the cells that express CLIC4 protein. After incubating the cells with 1 μM H_2O_2 or with both 1 μM H_2O_2 and 50 μM NAC for 24 h, the peroxidase activity increased specifically in CLIC4-KO cells compared to baseline. This elevation in peroxidase activity in response to H_2O_2 could explain the unchanged ROS and H_2O_2 levels in CLIC4-KO cells post-treatment with exogenous H_2O_2.

Using ThiolTracker violet and FACS analysis (Fig. S2*B*), there were no significant differences detected in GSH level between CLIC4-deficient and the WT 6DT1 cells. Altogether, these results support the concept that in the absence of CLIC4, cells live in a pro-oxidant internal environment.

Absence of CLIC4 impacts mitochondrial morphology and activity in 6DT1 cells

Specific components of mitochondrial respiration were further studied using Seahorse technology. At baseline, overall mitochondrial respiration did not differ among genotypes as measured by oxygen consumption rate (OCR) (Fig. 5, *A* and *B*). In contrast, oxygen consumption of CLIC4-KO cells was higher than the WT 24 h after exposure to 1 μM H_2O_2. Carbonyl cyanide p-trifluoromethoxy-phenylhydrazone, an uncoupler of mitochondrial oxidative phosphorylation, maximally stimulated oxygen consumption in CLIC4-KO cells treated with H_2O_2, suggesting these cells maintained higher spare respiratory capacity. The dependence on CLIC4 was supported by the return to WT levels of spare capacity when the CLIC4-deficient cells were reconstituted with CLIC4 lentivirus but not the empty vector. Shutting down mitochondrial respiration by inhibiting complex I and III with rotenone and antimycin A or reconstituting CLIC4 in CLIC4-KO cells did not reveal any differences in nonmitochondrial oxygen consumption among the genotypes. This result was further confirmed by using a second CLIC4-KO clone (Fig. S3*A*).

Extracellular acidification rate was also assayed by Seahorse to investigate the glycolytic capacity of cells to reveal any differences in other energy-producing pathways. Fig. S3*B* shows that there were no significant differences between the WT and CLIC4-KO cells in terms of glycolysis function.

Interestingly, electron microscopy images indicated that mitochondria in CLIC4-null cells were larger in diameter and rounder in shape than WT cells at baseline although this difference lost significance when WT cells were treated with H_2O_2 (as in Figs. 5, *C* and *D* and S3*C*). Treating the cells with NAC reversed the effect of H_2O_2 on mitochondrial morphology in both WT and CLIC4-deficient 6DT1 cells that are not treated or treated with H_2O_2.

Since CLIC4-KO cells demonstrated significant changes in mitochondrial morphologies and an increase in mitochondrial stress in response to H_2O_2, we investigated the mitochondrial activity further by measuring the mitochondrial membrane potentials.

Using TMRM (tetramethylrhodamine, methyl ester, perchlorate) on live cells, we found that the TMRM fluorescence as an indicator of mitochondrial membrane potential in 6DT1 cells lacking CLIC4 was substantially increased but only with H_2O_2 treatment. At baseline, mitochondrial membrane potential was not increased possibly through the activity of peroxidases or other antioxidants that mitigated the elevated ROS environment. Incubation with H_2O_2 also elevated TMRM fluorescence in WT cells to a lesser extent. Fluorescence in both genotypes was suppressed by NAC (Fig. 5*E*). The fluorescence of TMRM in response to H_2O_2 in 6DT1 cells was quantified using TECAN infinite M200 plate reader at an excitation of 488 nm and emission of 570 nm (Fig. 5*F*). The loss of CLIC4 was associated with an increase in several protein components of complex I, II, III and IV particularly 24 h post-H_2O_2 treatment that could be potentially contributing to the increased oxygen consumption in CLIC4-KO cells (Fig. S3*D*).

Altogether, these data suggested that the presence of CLIC4 contributed to regulating mitochondrial membrane potential, and in its absence, oxygen consumption and ROS production were increased. The consequences of these functions may also control mitochondrial morphology.

Apoptotic pathways are associated with H_2O_2 responses in the absence of CLIC4

Hydrogen peroxide increases mitochondrial activity in 6DT1 cells lacking CLIC4 and decreases cell viability potentially through an apoptotic pathway. Therefore, we examined the expression of essential proteins associated with apoptosis (Fig. 6*A*). Post-treatment with H_2O_2, cytochrome C protein was higher in lysates of CLIC4-KO 6DT1cells than treated WT cells. While the significance of elevated total cytochrome C is unclear, support favoring mitochondrial-dependent apoptosis came from the release of mitochondrial cytochrome C to the cytoplasm as seen in H_2O_2-treated CLIC4-KO 6DT1 cells (sg# 1) reconstituted with empty vector but not with CLIC4 (Fig. S4*E*). Unexpectedly, loss of CLIC4 was associated with reduced mitochondrial uncoupling protein 2 (UCP2) (Figs. 6, *A*–*C* and S4*A*) that functions to regulate oxidative stress and lowers mitochondrial membrane potential (51) in response to multiple stress signals as seen in WT cells where UCP2 increased after H_2O_2 treatment (Fig. 6, *A* and *B*). The reduction in UCP2 was also detected in 6DT1 CLIC4-KO clone sg# 2 (Fig. S4*A*) and was higher after reconstituting with CLIC4 lentivirus but not the empty vector (Fig. S4*C*). The reduction in UCP2 could decrease the mitochondrial response to oxidative stress and increase a cytotoxic outcome. The anti-apoptotic protein Bcl2 and the proapoptotic protein Bax were also substantially reduced in 6DT1 cells devoid of CLIC4. It is not clear why both are reduced similarly since Bcl2 is anti-apoptotic while Bax is proapoptotic. The consequence for the apoptotic process is not known but the reduction in both may indicate a general disruption of the mitochondrial integrity when CLIC4 is absent. Previously, it was shown that elevating CLIC4 cooperated with Bax to induce apoptosis, but the two

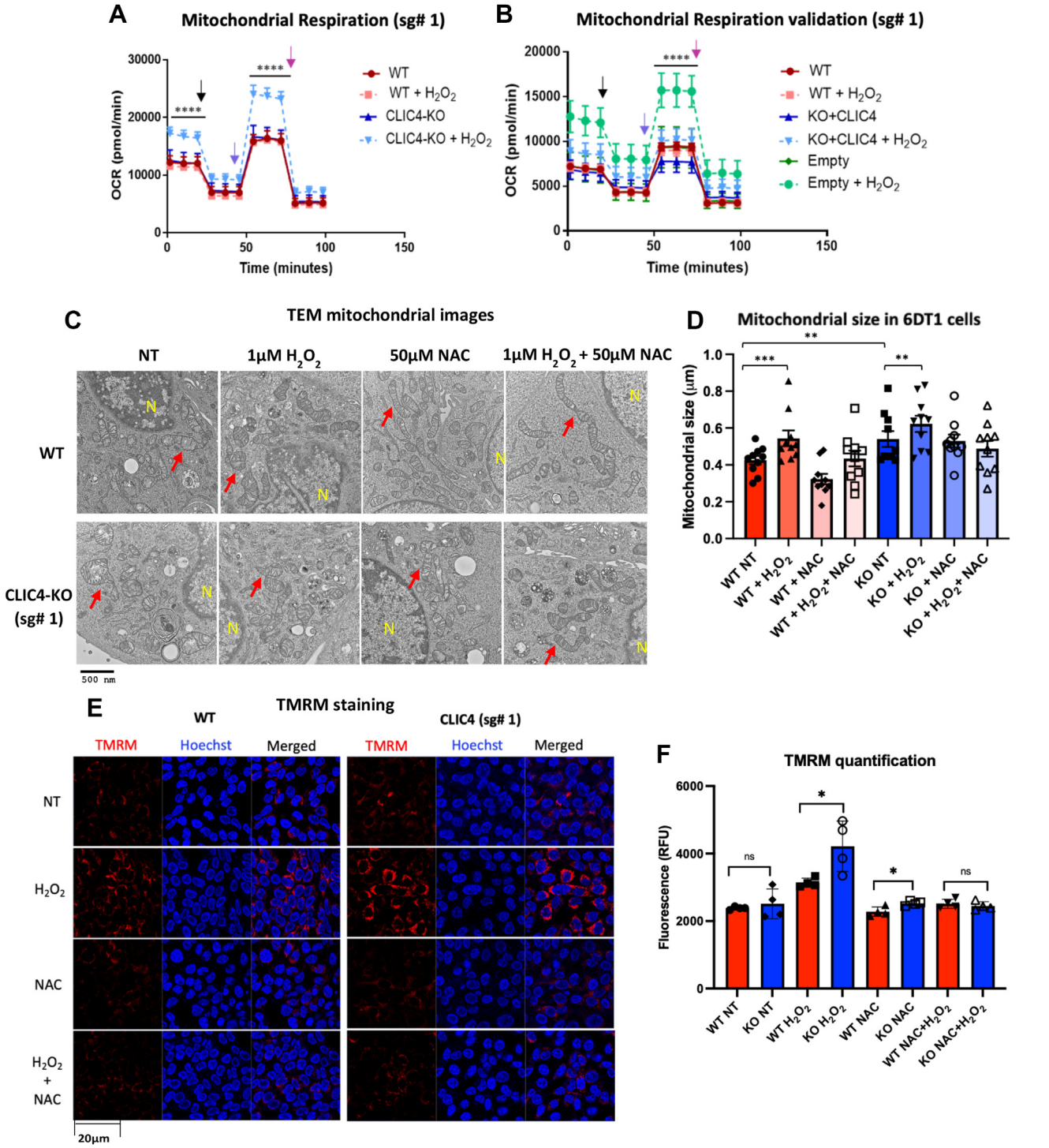

Figure 5. CLIC4 deficiency alters mitochondrial morphology and function in 6DT1 cells. *A* and *B*, CLIC4-WT, KO clone sg# 1, and KO+CLIC4 or control vector (Empty), untreated or treated with 1 μM H_2O_2 for 24 h, were incubated with prewarmed assay medium in a non-CO_2 incubator and 37 °C for 1 h and assayed for oxygen consumption rate (OCR) using the Agilent Seahorse XF kits. The *black downward arrow* indicates when Oligomycin was injected, the *purple arrow* is for FCCP, and the *pink arrow* is for Antimycin-A& Rotenone. The results were analyzed using prism pad 7 and data were presented as means ± SD of three independent experimental repeats. *C*, electron microscopy (EM) mitochondrial images at direct magnification of 5000× of CLIC4-WT, CLIC4-KO (clone sg# 1) untreated (NT) or are postincubated with 1 μM H_2O_2 with/without 50 μM NAC for 24 h. *D*, imageJ quantification of the mitochondrial diameters obtained by electron microscopy. *E*, 6DT1 CLIC4-WT, KO clone sg# 1, posttreated with 1 μM H_2O_2 with/without 50 μM NAC for 24 h, were incubated with 50 nM of TMRM for 30 min or with Hoechst (nuclear dye) for 5 min before processing for immunofluorescence confocal microscopy. *F*, 6DT1 CLIC4-WT and KO clone sg# 1 cells, postincubated with increasing concentrations of H_2O_2 for 24 h, were then incubated with 50 nM TMRM for 30 min to detect the mitochondrial membrane potential. *$p < 0.05$, **$p < 0.005$, ***$p < 0.0005$, and ****$p < 0.0001$. CLIC4, chloride intracellular channel-4; FCCP, carbonyl cyanide p-trifluoromethoxy-phenylhydrazone; NAC, N-acetyl cysteine; TMRM, tetramethylrhodamine, methyl ester.

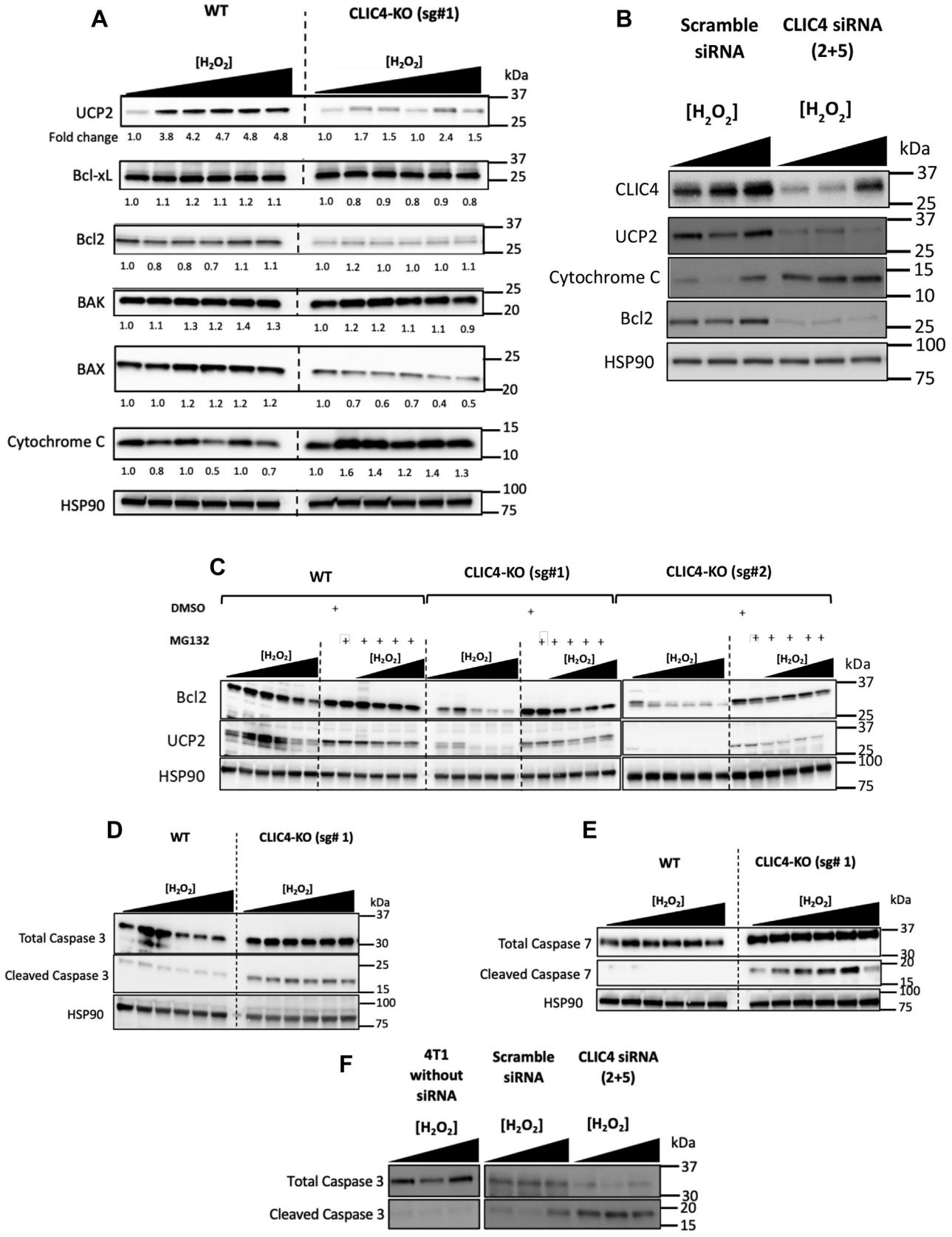

Figure 6. Mitochondrial apoptotic pathways are associated with H_2O_2 responses in the absence of CLIC4. *A*, CLIC4-WT or KO clone sg# 1 6DT1 cells were treated with varying concentrations of H_2O_2 (0, 0.1 μM, 0.5 μM, 1 μM, 10 μM, and 50 μM) for 24 h, and lysates were subjected to immunoblotting for expression of mitochondrial apoptotic BH3 proteins and UCP2. *B*, 4T1 cells transduced with scramble (negative control) or two CLIC4 siRNA (2 and 5 according to manufacturer's sequences) were then incubated with varying concentrations of H_2O_2 (0, 0.1 μM, 0.5 μM, 1 μM, 10 μM, and 50 μM of H_2O_2) for 24 h, and lysates were subjected to immunoblotting for expression of mitochondrial apoptotic BH3 protein, cytochrome C, and UCP2. *C*, CLIC4-WT or KO

proteins did not associate to accomplish this endpoint (50). As shown in Figure 3*A*, γH2AX is constitutively increased when CLIC4 is absent but in KO cells reconstituted with CLIC4, H_2O_2 treatment is required to elevate this DNA damage marker (Fig. S4, *A* and *C*). As an independent confirmation of these finding in 6DT1 breast cancer cells, we knocked down CLIC4 in the highly metastatic 4T1 breast cancer cell line with siRNA (Figs. 6*B* and S5). As shown in Figure 6*B*, reduction in CLIC4 protein was associated with loss of UCP2 and Bcl2 proteins and an elevation of total cytochrome C in response to H_2O_2.

Accumulation of high levels of ROS affects protein folding and increases the degradation of oxidized proteins (52, 53). Since the gene transcript levels for Bcl2 were not significantly changed (data not shown) after H_2O_2 treatment, we tested the idea that the loss may be posttranscriptional. Both Bcl2 and UCP2 levels were restored when CLIC4 KO cells were treated with both H_2O_2 in the presence of the proteasome inhibitor MG132 (Fig. 6*C*). CLIC4 has not been implicated in proteosome activation in response to a prooxidant environment and adds another dimension to the consequences of altered CLIC4 homeostasis.

The cleavage of caspases 3 and 7 are markers of mitochondrial-mediated cell death through an apoptotic pathway. Unlike WT 6DT1 cells, caspase 3 was cleaved in the two independent CLIC4 KO clones (Figs. 6*D*, and S4*B*) and the CLIC4 knockdown 4T1 cells treated with H_2O_2 (Fig. 6*F*). Reconstitution of clone sg# 1 with CLIC4 lentivirus but not the empty vector mitigated the cleavage of caspase 3 by H_2O_2. (Fig. S4*D*). Cleaved caspase 7 was also elevated in CLIC4-deficient 6DT1 cells treated with H_2O_2 (as shown in Fig. 6*E*).

The absence of CLIC4 in 6DT1 cells is associated with major transcriptional rewiring in response to oxidative stress

We isolated RNA and used RNAseq to investigate the transcriptional consequences of CLIC4 deficiency in 6DT1 cells (Fig. 7). Principle component analysis (PCA, Fig. 7*A*) showed the separation of the two groups [WT and CLIC4-KO 6DT1 cells] in the PC1. Among the KO cells, the untreated (NT) and the one treated with H_2O_2 also separated in the PC2 more effectively than the WT. Interestingly, gene expression differences based on genotype were far greater than the H_2O_2 treatment differences within each genotype. The Venn diagram (Fig. 7*B*) confirmed that nearly 8500 differentially expressed genes with significant p values of <0.05 distinguished the WT and CLIC4-KO cells without treatment, whereas treating the cells with 1 μM H_2O_2 resulted in 150 and 166 genes differentially expressed in the CLIC4-null cells and the WT 6DT1 cells, respectively.

A circle scatter plot (Fig. 7*C*) was used to sort out specific gene ontology (GO) pathways and the underlying genes that supported the plot (Fig. S6*A*) were documented. Consistent with the genotypic biological findings at baseline, predominant upregulation of pathways involved in response to oxidative stress, among which were endoplasmic reticulum stress and response to hydrogen peroxide characterized CLIC4-KO 6DT1 cells. Conversely, glutathione transferase activity– and oxidoreductase activity–related genes were relatively downregulated in the absence of CLIC4. Thus, this approach to transcriptional profiling was consistent with the experimentally defined biological consequences of deletion of CLIC4 from 6DT1 cells. From RNAseq data, five genes ($p < 0.05$, >1.5 fold), involved in regulating mitochondrial respiration, were expressed at substantially lower levels in CLIC4-KO relative to the WT 6DT1 cells without treatment. Post-treatment with H_2O_2 for 24 h, nine of those genes were lower in CLIC4-KO cells than WT (Fig. 7*D*). This response suggests a transcriptional programming is being invoked to both minimize the damage to the host while preserving the ability to generate energy and to survive. These differences are consistent with the vulnerability of CLIC4-deleted cells to mitochondrial toxicity after H_2O_2 treatment more broadly displayed by the cleavage of caspases, release of mitochondrial cytochrome C, and reduction in UCP2 and Bcl2 and Bax proteins.

Using the RNAseq data to generate gene set enrichment data, we investigated most relevant upregulated and downregulated pathways in Hallmark categories in gene set enrichment analysis (GSEA) pathway analysis. Some of the most constitutive differences were found in proapoptotic, inflammatory responses and the downregulation of protein secretion pathways (Fig. 7, *E*–*G*) in CLIC4-KO 6DT1 cells that could be reflecting the higher internal ROS levels and stress. The upregulation or downregulation of the Hallmark pathways of CLIC4-KO *versus* WT 6DT1 cells without treatment and some of the genes involved in oxidative phosphorylation were further validated with real-time PCR of three or four of the leading-edge genes of each pathway as in Fig. S6, *B*–*E*.

To confirm that the transcriptional differences detected between WT and KO cell types were CLIC4 rather than clonal based, the RNAseq was repeated comparing KO clone sg# 1 to a CLIC4 reconstituted twin using CLIC4 or empty vector lentiviruses. PCA (Fig. S7*A*) showed remarkable separation based on CLIC4 genotype whether treated or untreated with H_2O_2. As seen above for the H_2O_2-treated KO sg# 1 clone *versus* WT cells (Fig. 7), H_2O_2 treatment reiterated the GSEA leading edge inflammatory responses and apoptosis pathways favoring the KO empty vector clone over the reconstituted CLIC4 clone (Fig. S7, *B* and *C*), suggesting the presence or absence of CLIC4 determines these responses.

CLIC4-null mammary tumors are smaller and more necrotic

Many chemotherapeutic drugs generate ROS in cancer cells or contribute to the accumulation of ROS by inhibiting the cellular detoxification systems (54).

clones sg# 1 and sg# 2 6DT1 cells were treated with 0, 0.1 μM, 0.5 μM, 1 μM, 10 μM, and 50 μM of H_2O_2 for 24 h or with 0, 0.5 μM, 1 μM, 10 μM, and 50 μM of H_2O_2 and 15 μM MG132 for 24 h before being lysed and immunoblotted for investigating the expression of the antiapoptotic protein Bcl2 and the mitochondrial ROS moderator UCP2. *D* and *E*, CLIC4-WT or KO clone sg# 1 6DT1 cells were treated with 0, 0.1 μM, 0.5 μM, 1 μM, 10 μM, and 50 μM of H_2O_2 or (*F*) 4T1 cells transduced with scramble (negative control) or *Clic4* siRNA (2 + 5) treated with 0, 1 μM, and 10 μM of H_2O_2 for 24 h, and lysates were subjected to immunoblotting for expression of total and cleaved caspases 7 and caspase 3. CLIC4, chloride intracellular channel-4; ROS, reactive oxygen species.

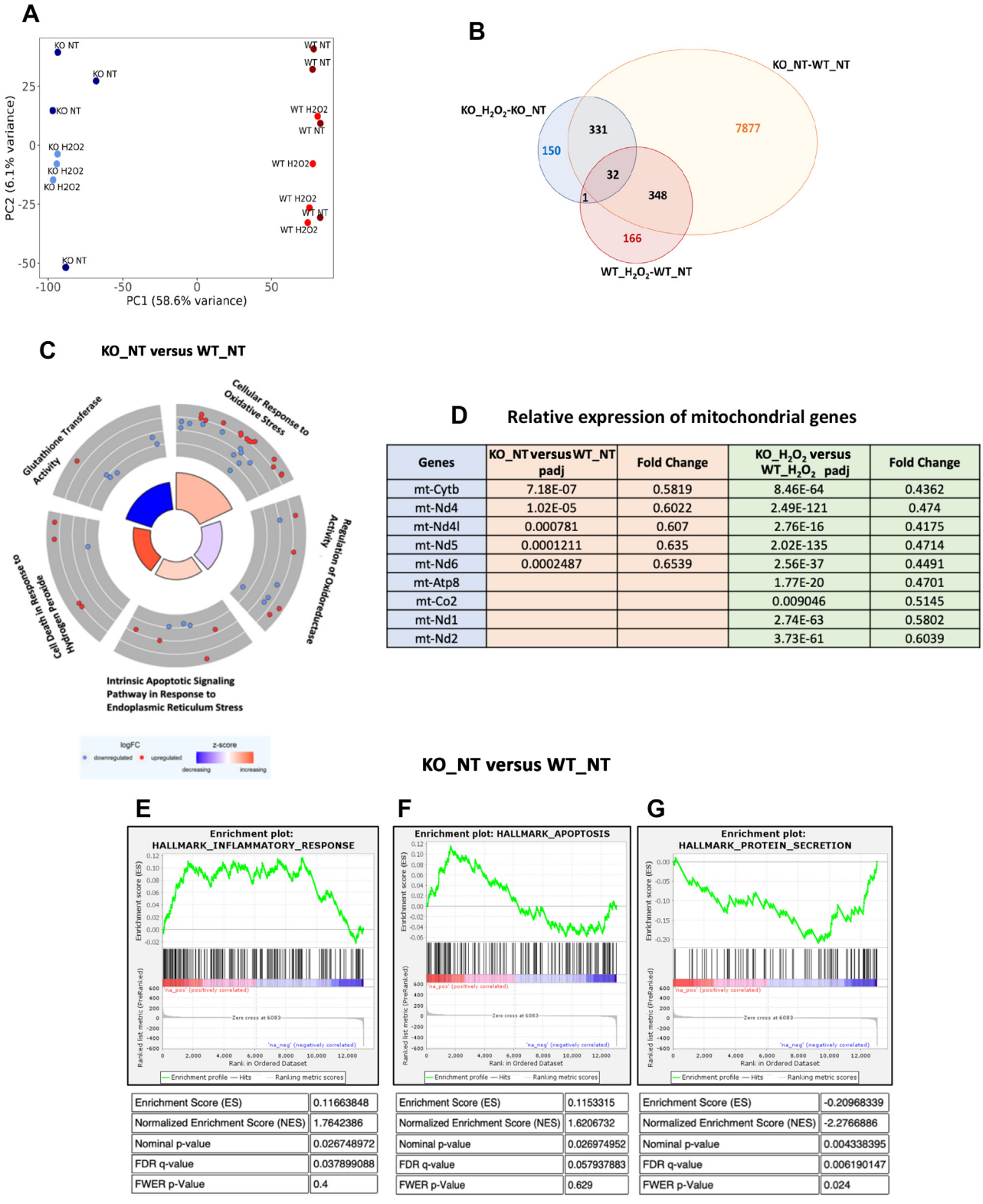

Genes	KO_NT versus WT_NT padj	Fold Change	KO_H_2O_2 versus WT_H_2O_2 padj	Fold Change
mt-Cytb	7.18E-07	0.5819	8.46E-64	0.4362
mt-Nd4	1.02E-05	0.6022	2.49E-121	0.474
mt-Nd4l	0.000781	0.607	2.76E-16	0.4175
mt-Nd5	0.0001211	0.635	2.02E-135	0.4714
mt-Nd6	0.0002487	0.6539	2.56E-37	0.4491
mt-Atp8			1.77E-20	0.4701
mt-Co2			0.009046	0.5145
mt-Nd1			2.74E-63	0.5802
mt-Nd2			3.73E-61	0.6039

Enrichment Score (ES)	0.11663848
Normalized Enrichment Score (NES)	1.7642386
Nominal p-value	0.026748972
FDR q-value	0.037899088
FWER p-Value	0.4

Enrichment Score (ES)	0.1153315
Normalized Enrichment Score (NES)	1.6206732
Nominal p-value	0.026974952
FDR q-value	0.057937883
FWER p-Value	0.629

Enrichment Score (ES)	-0.20968339
Normalized Enrichment Score (NES)	-2.2766886
Nominal p-value	0.004338395
FDR q-value	0.006190147
FWER p-Value	0.024

Figure 7. Loss of CLIC4 in 6DT1 cells is associated with major transcriptional rewiring associated with response to oxidative stress. *A*, principal component analysis (PCA) using global expression profiles (∼13K genes selected as described in the Experimental procedures) of CLIC4-WT and KO clone sg# 1 untreated (NT) cells or treated with 1 μM H_2O_2 for 24 h separated by genotype and treatment. *B*, Venn diagram showing the numbers of overlapping and distinct sets of differentially expressed genes (DEGs) in CLIC4-WT or KO clone sg# 1 6DT1 cells with or without H_2O_2 treatment. *C*, gene ontology (GO) circle plot for DEGs between CLIC4-WT and CLIC4-KO 6DT1 cells without treatment and the over-represented GO terms. The *outer ring* shows a scatter plot of the log2 fold change for each gene under the GO term; *red dots* indicate the upregulated and *blue* the downregulated genes. The *inner ring* is a bar plot, where the height of the bar indicates the significance of the GO term enrichment (−log10 *p*-value), and the color corresponds to the z-score: *blue*, decreased; *red*, increased; and *white*, unchanged. *D*, Differentially Expressed Mitochondrial Genes (DEMGs, $p < 0.05$, >1.5 fold) in CLIC4-KO compared to CLIC4-WT 6DT1 cells without treatment (NT) or treated with 1 μM H_2O_2 for 24 h. *E–G*, GSEA leading edge enrichment plot of three significantly regulated hallmark pathways in untreated CLIC4-KO clone sg# 1 compared to CLIC4-WT 6DT1 cells untreated. *p* value of 0.0 indicates an actual *p* value of less than 0.01. CLIC4, chloride intracellular channel-4; GSEA, gene set enrichment analysis.

CLIC4 is required to maintain mitochondrial function

Incubating 6DT1 cells with increasing concentration of epirubicin or oxaliplatin was cytotoxic in a dose range of 0.1 to 10 μM, but cells lacking CLIC4 were significantly more sensitive (Fig. S8, *A* and *B*). Epirubicin which is an anthracycline that induces mitochondrial ROS generation (54) and to lesser extent oxaliplatin that is an alkylating drug that induces ROS production *via* NOX1 activation (55) increased the expression of CLIC4 (Fig. S8, *C* and *D*). Other chemotherapeutic drugs such as paclitaxel that generates ROS through enhancing the activity of NADPH oxidases (56) and tipifarnib that decreases the intracellular ROS (57) did not differentially affect the cell viability or CLIC4 protein expression in any of the genotypes (Fig. S8, *E–H*). Our data suggested that the viability of CLIC4-KO 6DT1 breast cancer cells was sensitive to multiple stimuli that elevate ROS, and the induction of CLIC4 was highly responsive to the elevation of mitochondrial ROS.

Growth and viability are impaired for 6DT1 tumors lacking CLIC4

Injecting CLIC4-deficient 6DT1 cancer cells into FVB mice resulted in the formation of tumors with significantly lower masses than the WT tumors that formed (Fig. 8*A*). It is well known that cell death, and in particular necrosis, is commonly observed in regions of solid tumors as a result of inadequate vascularization and subsequent metabolic stress and hypoxia (58). Herein, we observed a significant increase in necrotic/apoptotic tumor foci in CLIC4-KO tumors as shown in Figure 8*B* and the H&E staining in Figure 8*C* that was further

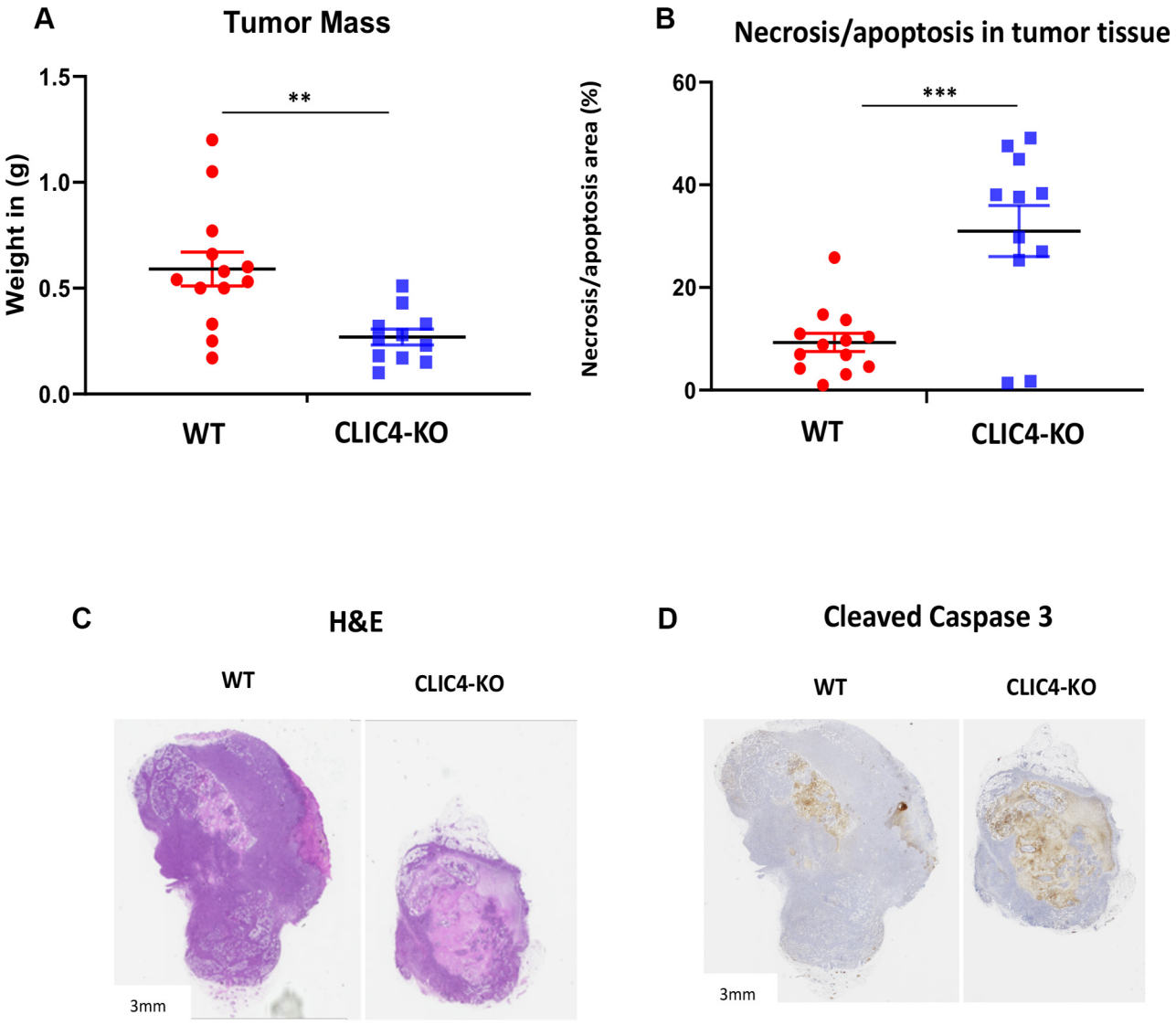

Figure 8. Growth and viability are impaired for 6DT1 tumors lacking CLIC4. 1×10^5 6DT1 cells either WT or KO for CLIC4 were injected into the mammary fat pad of *Clic4*-WT FVB female mice. The primary tumors were extracted after 3 weeks, weighed, fixed in formalin, and sectioned for histology. WT, n = 13 and KO, n = 11. *A*, mean weight of CLIC4-WT and CLIC4-KO tumors. Each dot is an individual tumor. *B*, mean and individual variation of necrotic/apoptotic tissues in CLIC4-WT and KO clone sg# 1 tumors that are H&E stained. The area of necrosis was subtracted from the total area of each tumor and converted to percentages. Each square is an individual tumor. $^{**}p < 0.005$ and $^{***}p < 0.0005$. *C*, representative H&E staining of a tumor from each genotype. Poorly stained anuclear areas were considered necrotic/apoptotic foci. *D*, immunohistochemistry using staining of the necrosis marker–cleaved caspase 3 confirms necrotic/apoptotic regions. CLIC4, chloride intracellular channel-4.

confirmed with cleaved caspase 3 staining as an apoptosis/necrosis marker as in Figure 8*D*.

All together, these results suggested that CLIC4 protects cancer cells against oxidative damage generated in the *in vivo* environment.

Discussion

In this breast cancer model system, our data show that CLIC4 is an important regulator of internal ROS generation and serves to protect cell viability against external prooxidant exposures, including chemotherapeutic agents. This is consistent with the discovery of enzymatic oxidoreductase activity for recombinant CLIC4 protein *in vitro* (23) and with its membership in the GST superfamily of antioxidants. Since CLIC1 and CLIC2 share oxidoreductase activity with CLIC4 (23), this activity may represent important fundamental cellular functions of the CLIC family and is consistent with the extensive conservation of CLIC homologs, orthologs, and paralogs through the vertebrate and invertebrate phyla (21).

Results with multiple CLIC4-KO clones and CLIC4 reconstitution experiments firmly support our conclusions that CLIC4 is an integral part of the cellular antioxidant repertoire. Without CLIC4, these breast cancer cells compensate by using other antioxidants to overcome a prooxidant environment. Our *in vivo* data indicate that tumors lacking CLIC4 do not achieve maximal weight and have extensive necrosis. Thus, a drug targeting CLIC4 could enhance prooxidant therapy in diseases such as cancer (59). In fact, high expression of CLIC4 has been associated with poor outcome in multiple human cancers as shown by the Kaplan–Meier plots presented on public databases (46) perhaps suggesting that CLIC4 is protective against oxidative processes that might otherwise restrict tumor growth. Beyond the 6DT1 and 4T1 breast cancer models, CLIC4 expression is associated with transforming growth factor-beta signaling and could mediate tumor growth through modulation of ROS as previously suggested (33). CLIC4 downregulation enhanced apoptosis in head and neck cancer cells (60), C6 glioma cells (59), and U251 glioma cells (61). In all cases, a mitochondrial apoptotic pathway was implicated. Paradoxically, CLIC4 elevation has also been associated with mitochondrial-mediated apoptosis in non-cancer cells in LPS/c-myc–induced neuronal cell death (62), endothelial cell apoptosis induced by LDL lipids (63), and pancreatic β-cell apoptosis induced by cytokines (64), suggesting that the level of CLIC4 and the physiological state of the cell type involved were important to determine the biological outcome.

More than 2 decades ago, CLIC4 was recognized as a resident mitochondria protein and localized to the mitochondrial inner membrane and the matrix of keratinocytes using EM immunogold (50). While this localization has not been confirmed by other methods, our functional studies indicate that it is possible that inner membrane is the site of action for CLIC4. CLIC4 played a critical function in maintaining mitochondrial membrane potential in L929 cells depleted of mitochondrial DNA (65). More recently, mitochondrial CLIC4 has been implicated in two human diseases, ethylmalonic encephalopathy (66) and Parkinson's disease (67). We showed that in the absence of CLIC4, intracellular superoxide and H_2O_2 levels were elevated, there was a high ROS environment, and cells were vulnerable to additional prooxidant exposures. Through Seahorse, we found that H_2O_2 treatment of CLIC4-deleted cells produced excess mitochondrial OCR, and selected dyes revealed elevated mitochondrial superoxide production and high mitochondrial membrane potential. Together, these findings suggested that mitochondria were functionally overactive in the absence of CLIC4. Thus, specific levels of CLIC4 were necessary to maintain normal mitochondrial homeostasis. Exposure to H_2O_2 in the absence of CLIC4 decreased cell viability in a process that modeled mitochondrial-mediated apoptosis characterized by the release of mitochondrial cytochrome C and cleavage of the proapoptotic caspases 3 and 7. Furthermore, Bcl2, Bax, and UCP2 levels decreased due to enhanced degradation, suggesting that a cascade of mitochondrial events followed a prooxidant stress with the loss of CLIC4.

Strikingly, the loss of CLIC4 was associated with abundant transcriptional changes, some of which were likely associated with the high ROS related to the mitochondrial impact, but others may also be a consequence of CLIC4-mediated cellular functions in other pathways (68, 69). Our transcriptional analysis focused on proapoptotic and mitochondrial pathways, disclosing multiple expression changes that reflect the biology we are reporting. RNAseq of CLIC4-KO cells detected reductions in the expression of selected mitochondrial genes that was accentuated with H_2O_2 treatment that could be a protective response to high ROS, upregulated endoplasmic reticulum stress, or downregulation of protein secretions pathway (70, 71). Nevertheless, some key proteins in the electron transport complexes remained elevated presumably supporting the OCR of the CLIC4-KO cells. CLIC4, either directly or indirectly, also contributes to the structural integrity of the mitochondria as those lacking CLIC4 are enlarged in diameter. Additional work will be required to understand the structural basis and functional consequences of these morphological changes that can also be a sign of oxidative stress.

The wider conclusion from this study is that CLIC4 contributes important homeostatic properties to mitochondrial functions and should be considered as a candidate molecule for focus in human diseases of mitochondrial origin including cancer.

These data confirm that CLIC4 protects host cells from a prooxidant environment, regulates mitochondrial function, and reduces the apoptotic response that follows exposure to oxidative stress. However, at this time, we cannot distinguish the intrinsic CLIC4 biological function or functions that accomplish these tasks. CLIC4 has innate oxidoreductase activity and putative ion transport functions, both or either of which could be important in its antioxidant and mitochondrial activity. As far as we know, changes in the distribution of the mitochondrial ionic milieu attributable to CLIC4 have not been reported. As an oxidoreductase, we show that CLIC4

contributes to a complex antioxidant defense system that could also function inside mitochondria along with, for example, SOD2 and the glutaredoxins in the inner mitochondrial space or/and matrix (72). CLIC4 may also have an oxidoreductase function in the cytosol as shown for secreted paralog CLIC3 that reduces transglutaminase 2 in the microenvironment of medulloblastoma cells altering the stiffness of the extracellular matrix (73). By a mechanism, yet to be elucidated, the presence of CLIC4 also retards the proteolysis of mitochondrial proteins such as UCP2 and Bcl2 raising yet another potential function that contributes to the cellular response to stress. This multitude of possibilities could underly the observation that CLIC4 can maintain mitochondrial integrity in cells completely lacking mitochondrial DNA (65). Future studies will likely require detailed analysis of isolated mitochondria coupled with mutagenesis and biophysical measurements to unravel the specific CLIC4 function necessary for its vital role in mitochondrial maintenance and protection from oxidative stress.

Experimental procedures

Cell cultures and CRISPR/Cas9

The murine breast cancer cell line 6DT1 from FVB mice has been previously described (74). Cells were cultured in 150 × 25 mm polystyrene tissue culture plates (Cat# 353025, Falcon) in phenol-red Dulbecco's modified Eagle's medium (DMEM, Cat# 11995065, ThermoFisher scientific) containing 10% fetal calf serum (Cat# 100-106, GeminiBio or Cat# A4766801, Gibco), Hepes (Cat# 15630080, ThermoFisher), and penicillin-streptomycin (Cat# 15140163, Gibco). They were grown at 5% CO_2, 37 °C until they reached at least 80% confluency before being used. The CLIC4-KO clones were generated by CRISPR Cas9. Briefly, parental 6DT1 cells were infected with lentiviral particles containing CRISPR/Cas9 and sgRNA targeting murine *Clic4* (caccgCTTCAACAGCGAAGTCAAGA and caccgTTGACGAAGAGCTCGATGAG). Single cell clones were selected with puromycin and CLIC4 deletion was confirmed by immunoblot.

Animals

Mouse studies were performed under protocol LCBG-038 and LCBG-035 approved by the National Cancer Institute Animal Care and Use Committee.

1×10^5 6DT1 WT (n = 13) and KO (clone sg# 1) (n = 11) cells were injected subcutaneously into the mammary fat pad of syngeneic FVB/N female mice. After 3 weeks, tumors were excised and weighed and fixed in 10% neutral buffered formalin (Cat# 5735, ThermoFisher) for sectioning.

Cell viability and proliferation assay

6DT1 cells were harvested using Trypsin-EDTA (Cat# 25200056, Gibco), and 5000 cells were replated in 96-well plates (Cat# 353072, Life Sciences) for 24 h. Growth medium was switched to phenol red–free DMEM (Cat# 21041025, Gibco) containing 10% fetal bovine serum and penicillin-streptomycin at a final volume of 100 μl per well. After 2 h of equilibration, the cells were treated with different concentrations of H_2O_2 (Cat# H1009, Sigma Aldrich), catalase (Cat# C1345, Sigma Aldrich), or NAC (Cat# A9165, Sigma Aldrich) for 24 h Ten microliters of CCK-8 (Cat# CK-04-13 Dojindo Molecular Technologies) was added to control and treated wells for 1 to 2 h, and absorbance was measured using the Tecan 200 plate reader at 450 nm. This procedure was also performed on the preincubated 6DT1 cells with different concentrations of epirubicin (Cat# E-8000, LC Laboratories) or oxaliplatin (Cat# O-7111, LC Laboratories) or paclitaxel (Cat# P-9600, LC Laboratories) or tipifarnib (Cat# T-9104, LC Laboratories) chemotherapeutic drugs for 24 h.

In some experiments, cells were treated with different concentrations of H_2O_2, catalase, or NAC for 24 h and assayed for DNA content with the CyQuant cell proliferation assay (Cat# C35006, ThermoFisher Scientific) following manufacturer's instructions. Fluorescence intensity was measured using the Tecan 200 plate reader at an excitation of 485 nm and emission of 530 nm. All experiments were performed in triplicate wells for each treatment condition and repeated three times.

Confocal microscopy and superoxides/ROS detection

6DT1 cells were seeded in plastic chamber slides (Cat# 80446, Ibidi) at a density of 50,000 cells. After 24 h, the cells were switched to phenol red–free complete DMEM media and treated with H_2O_2 and catalase or NAC for 24 h.

Postincubation, the cells were incubated with 0.5 μM Mito-Tracker Orange CMTMRos (Cat# M7510, Molecular Probes) for 30 min at 37 °C and 5% CO_2. Stained cells then were washed with ice cold 1× PBS (Cat# RGE-3210, KD Medical) and fixed with ice cold 4% paraformaldehyde (Cat# 15710, Electron Microscopy Science) for 15 min at room temperature with gentle agitation. Fixed cells were permeabilized for 10 min at room temperature with 5% bovine serum albumin (Cat# A3311, Sigma Aldrich) and 0.1% Triton X-100 (Cat# 1610407, Bio-Rad). After washing and blocking with 5% bovine serum albumin made in 1× PBS for 1 h, CLIC4 antibody (Cat# 12644, Cell Signaling Technologies) was applied at 1:200 dilution. Slides were stored at 4° for 24 h and then overlaid with Alexa-fluor 488–labeled secondary antibody (Cat# A-11034, ThermoFisher Scientific) for 1 h. Coverslips were applied with antifade mounting media along with DAPI (Cat# H-1200-10, Vector laboratories) or Hoechst (Cat# H3570, IFE Technologies) at 1:5000 dilution for 5 min at room temperature with gentle agitation. Slides were viewed using a Zeiss confocal microscope and a 63× oil-immersion objective. Images of cells treated only with primary or secondary antibodies were viewed for nonspecific fluorescence. 1×10^6 6DT1 cells in each well of the 6-wells plate (Cat# 353046, Falcon) were left untreated or treated with 1 μM H_2O_2 and/or 50 μM NAC in complete phenol-free DMEM medium for 24 h at 37 °C and 5% CO_2. After a PBS wash, plates were incubated with a final concentration of 3 μM of CellROX green (Cat# C10444, ThermoFisher Scientific) or 5 μM CM-H2DCFDA (Cat# C6827, ThermoFisher Scientific) for 30 min and examined by

confocal microscopy *in situ* or isolated cells evaluated by FACS on a BD LSR Fortessa SORPII at 10,000 cells per minute. MitoSOX Red (Cat# M36008, ThermoFisher Scientific) dissolved in dimethyl sulfoxide at a final concentration of 2 μM per 1 × 10^6 cells in 2 ml of HBSS buffer (Cat# 21-022-CV, Corning Cellgo) was assayed similarly.

Cell preparation for TEM imaging and mitochondrial measurements

The cultured 6DT1 cells untreated or treated with 1 μM H_2O_2 or 50 μM NAC or with both for 24 h in 6-wells plate were then fixed for at least 2 h in glutaraldehyde (2% v/v) cacodylate buffer (0.1 M, pH 7.4) in preparation for thin-sectioned EM analysis as described in (43). Following fixation, the cells were washed with ddH_2O before being incubated with osmium tetroxide (1% v/v) for 1 h. The cells were then washed two times with ddH_2O and one time with acetate buffer (0.1 M, pH 4.5) before *en block* stained in 0.5% w/v uranyl acetate (0.5% v/v) in acetate buffer (0.1 M, pH 4.5) for 1 h. The cells were dehydrated with multiple washes of EM-graded ethanol at 35%, 50%, 75%, 95%, and 100% consecutively. The cells were then washed with pure epoxy resin 3 times over 12 h, embedded, and warmed in a 55 °C oven to cure for 48 h. Once cured, the resin blocks were separated from the plate and examined under an inverted microscope to select an area with a considerable number of cells. The preferred area was removed from the block, trimmed, and thin sectioned using an ultramicrotome equipped with a diamond knife. The thin sections were mounted onto copper mesh grids for counter staining with uranyl acetate and lead citrate. The grids were then carbon coated in a vacuum evaporator. Once carbon coated, the grids were prepared to be scanned and imaged. The Hitachi Electron microscope (H7650) operated at 80 kv with a CCD camera captured the digital images.

Mitochondrial diameters of ten randomly selected images of each genotype and condition were obtained as follows: using ImageJ, the area of the mitochondrion was obtained and converted to diameter (μM). Then, the total measurements were averaged, and one final diameter was obtained for each genotype and condition.

Mitochondrial isolation

Mitochondrial and cytosolic fractions from 6DT1 cells (reconstituted with CLIC4 or empty vector) were performed by using the Mitochondria Isolation Kit for Cultured Cells (Cat# 89874, ThermoFisher). Following manufacturer's instructions, 2 × 10^7 cells were lysed in a hypotonic buffer and isolated mitochondria were released using Dounce homogenizer (40 strokes) in mitochondrial buffer on ice. The isolated mitochondrial pellet was washed with mitochondrial buffer and lysed using 2% CHAPS in 1× PBS. The total mitochondrial and cytosolic proteins were quantified using BCA protein quantification kit (Cat# 23225, Pierce).

Immunoblotting

Cultured cells were treated with whole cell lysis buffer (Cat# 9803, Cell Signaling Technologies) containing 1× protease and phosphatase inhibitors (Cat# 78441, ThermoFisher Scientific) and collected after scraping on ice. Total protein concentration of the lysates was quantified using the BCA protein quantification kit (Cat# 23225, Pierce), and 20 μg of the total protein was loaded onto precast 4 to 20% tris–glycine protein gels (Cat: 5671094, Bio-Rad Laboratories). Following electrophoresis, protein bands were transferred to a nitrocellulose membrane (Cat# 1620168, Bio-Rad) and incubated with primary antibodies for 24 h at 4 °C with rocking and further incubated with the appropriate secondary horseradish peroxidase–conjugated antibodies for 1 h at room temperature with agitation. Then, blots were developed with chemiluminescence substrates (Cat# 3407 and 34076, ThermoFisher Scientific) using the ChemiDoc imaging system (Cat# 12003153, Bio-Rad).

Immunoblots were performed with antibodies from Cell Signaling Technologies against CLIC4 (Cat# 12644S), CLIC1 (Cat# 53424S), SOD1 (Cat# 37385S), SOD2 (Cat# 13141S), catalase (Cat# 12980S), histone H2A.X (yH2Ax) (Cat# 7631S), HSP90 (Cat# 4877S), beta-actin (Cat# 4970S), lamin A/C (Cat# 4777S), Bcl-xL (Cat# 2764S), Bak (Cat# 12105S), Bcl2 (Cat# 3498S), Bax (Cat# 5023S), cytochrome C (Cat# 11940S), UCP2 (Cat# 89326S), caspase 3 (Cat# 14220S), caspase 7 (Cat# 12827S), and vinculin (Cat# 13901S). Anti–GST-Omega 1 was from Invitrogen (Cat# PA5-83383). OxPhos Rodent WB Antibody Cocktail (Cat# 45-8099, ThermoFisher).

Immunoblots were quantified using ImageJ and normalized to the loading controls (HSP90, vinculin).

RNA isolation and sequencing

Tetraplicates of H_2O_2 treated or control 6DT1 cells of different genotypes were lysed after 24 h with RLT lysis buffer containing 1% beta-mercaptoethanol. RNA was extracted using the QIAcube as per instructions (RNeasy kit from Qiagen). mRNA sequencing was performed using Illumina Sequencing Technology by the Sequencing Facility at the Frederick National Laboratory for Cancer Research and analyzed by the CCR Collaborative Bioinformatics Resource group. Poly-A–selected mRNA libraries were generated using the Illumina TruSeq v4 stranded library protocol. Samples were pooled and paired end sequenced on the Illumina HiSeq 4000 in a single lane.

RNAseq data analysis

Sixteen mRNA-Seq samples were pooled and sequenced on NextSeq using Illumina TruSeq Stranded mRNA Library Prep and paired-end sequencing. The samples have 25 to 38 million pass filter reads with more than 94% of bases above the quality score of Q30. The RNA sequences were aligned to the mouse reference genome mm10 using STAR (75) and RSEM (76) to obtain RNA expression, and the differentially expressed genes were found by using DESeq2 (77, 78) to compare RNA expression between two conditions. Comparisons were

CLIC4-KO *versus* CLIC4-WT (WT), meaning CLIC4-KO compared to CLIC4-WT 6DT1 cells or CLIC4+Empty (KO 6DT1 cells transduced with lentivirus with empty vector) *versus* KO+CLIC4 (cells reconstituted with lentiviral particles to express CLIC4) that are untreated (NT) or treated with 1 μM H_2O_2 for 24 h.

Based on the statistics from the DESeq2 analysis, GSEA (79) was developed, and pathway interpretation through the Hallmarks collection was performed. Results were filtered based on adjusted *p*-value then sorted on normalized enrichment score.

PCA of samples was done using a singular value decomposition of normalized and scaled RNAseq counts (R princomp function). Prior to the PCA analysis, low expression genes were removed (counts-per-million less than one in all samples) and the raw counts were normalized with a variance-stabilizing transformation using the DESeq2 method (77). A Venn diagram was generated with the R Venn Diagram library (80), selecting genes with a nominal *p*-value less than 0.05. The top significant genes (up to 1000 genes) were used for the GO enrichment analysis in DAVID (81). Directionality of gene expression change in a gene set was represented with a z-score (82) defined based on the number of upregulated and downregulated genes as the ratio of $(N_{up} - N_{down})/sqrt(N_{total})$. Selected over-represented pathways were visualized with a circle plot using the R GOplot library (82). The analyses were performed using the R programming language [https://cran.r-project.org/], where the Venn diagram and PCA plot were generated using R version 3.5.1 and the NIDAP environment (the NIH Integrative Analysis Platform) [https://nidap.nih.gov], and the GO circle plots were generated using R 3.6.3 and RStudio [https://www.rstudio.com/].

Reverse transcription PCR analysis

Total RNA was isolated from cultured 6DT1 cells using RLT RNeasy QIAcube platform (Qiagen) and on-column DNA digest (Qiagen, 79254) according to manufacturer's protocol (Invitrogen, 15596018). Complementary DNA synthesis and real-time PCR analysis were conducted as described previously (83). Primers for CLIC4 were as follows: forward: CTCTTCGTCAAGGCCGGAAG and reverse: CGGTTGT GACACTGAACACG, purchased from Integrated DNA Technologies, and primers for Gapdh were as follows: forward: 5′-CATGGCCTTCCGTGTTCCTA-3′ and the reverse: 5′-GCGGCACGTCAGATCCA-3′, purchased from Qiagen. All the other primers used for this study are commercially available QuantiTect Primers purchased from Qiagen, Cat# 249900.

siRNA transfection of 4T1 cells

4T1 cells were cultured in 6-wells plate and transfected with a total concentration of 30 nM of specific *Clic4* siRNA (Cat# 1027416, Qiagen) or with a mix of two siRNAs (15 nM each) or with 20 nM of scramble as a negative control (Cat# 1022076 or 1027310, Qiagen) using HiPreFect transfection reagent (Cat# 301705, Qiagen) in serum-free DMEM medium according to manufacturer's instructions. After 24 h, the transfection medium was replaced with fresh complete DMEM media, and the cells were left in culture for 3 days. The expression level of CLIC4 protein in 4T1 cells treated with scramble or *Clic4*-mouse siRNA was then assessed with immunoblotting.

ROS detection and measurements

1×10^6 6DT1 cells in each well of the 6-well plates (Cat# 353046, Falcon) were left untreated or treated with 1 μM H_2O_2 and/or 50 μM NAC in complete phenol red–free DMEM medium for 24 h at 37 °C and 5% CO_2. After a 1× PBS wash, plates were incubated with a final concentration of 3 μM of CellROX green (Cat# C10444, ThermoFisher Scientific) or 5 μM CM-H2DCFDA (Cat# C6827, ThermoFisher Scientific) for 30 min and examined by confocal microscopy *in situ*, or isolated cells were evaluated by FACS on a BD LSR Fortessa SORPII at 10,000 cells per minute.

MitoSOX Red (Cat# M36008, ThermoFisher Scientific) dissolved in dimethyl sulfoxide at a final concentration of 2 μM per 1×10^6 cells in 2 ml of HBSS buffer (Cat# 21-022-CV, Corning Cellgro) was assayed similarly.

Hydrogen peroxide quantification was determined using Amplite colorimetric hydrogen peroxide assay kit (Cat# 11500, AAT Bioquest) following the manufacturer's protocol.

Briefly, cells were harvested and placed into phosphate buffer (pH 7.4). After spin-down of cell debris, 50 μl of supernatant was loaded with 50 μl of working solution. Following a 30 min incubation, the absorbance at 650 nm was then measured in clear bottom 96-well plates (Cat# 137101, ThermoFisher Scientific) using the TECAN infinite M200 microplate reader.

Assessment of peroxidase activity with Amplex Red peroxidase assay kit (Cat# 22188, ThermoFisher Scientific) was performed according to manufacturer's instructions, using the fluorescence of resorufin at an excitation of 570 nm and emission of 585 nm.

Thiol-tracker Violet was used to quantify the GSH content in WT (CLIC4-WT) or CLIC4-KO 6DT1 cells. The cells were plated on plastic chamber slides (Cat# 80446, Ibidi) at a density of 50,000 cells per well and incubated overnight at 37 °C in phenol red–free complete medium. Cells were then treated with 1 μM H_2O_2 or 50 μM NAC or both and reincubated for another 24 h and stained with 20 μM ThiolTracker Violet dye for 20 min in the dark at 37 °C. Cells then were washed with DPBS and harvested with trypsin-EDTA and processed for FACS analysis.

Catalase activity measurement

Catalase activity in 6DT1 cells was determined using a colorimetric Catalase Activity Assay Kit (Cat# ab83464, Abcam) according to the manufacturer's instructions. The absorbance of the samples was assessed using TECAN infinite M200 at 570 nm.

Seahorse analysis

A Cell Mito-stress Test (Cat# 103708-100, Agilent) was performed based on manufacturer's instruction on the Agilent seahorse XFe96 analyzer. 6DT1 cells were plated on sterile XFp24 and 96-well plates in duplicate at 4×10^4 total cells per well and serially stimulated with 1 μM oligomycin, 0.5 mM carbonyl cyanide 4-(trifluoromethoxy) phenylhydrazone, and 2 μM rotenone. Respiratory parameters calculated included basal OCR, OCR for ATP production, total respiratory capacity, spare respiratory capacity, and nonmitochondrial respiration. In addition, a glycolysis-stress test (Cat# 103710-100, Agilent) was performed following manufacturer's protocol. Briefly, after 24 h incubation, the medium was changed to assay medium (XF base medium DMEM supplemented with 2 mM glutamine), and 6DT1 cells were incubated in a non-CO_2 incubator at 37 °C for 1 h before the assay. Injections of glucose (10 mM final), oligomycin (0.5 μM final), and 2-DG (100 mM final) were diluted in the assay medium and loaded into ports A, B, and C, respectively. The extracellular acidification rate was measured under basal conditions followed by the sequential addition of 10 mM glucose, 0.5 μM oligomycin, and 50 mM 2-DG (Glu > Oli > 2-DG). Assay medium was injected instead of glucose, oligomycin, and 2-DG serving as the control.

The mito-stress test report and the glycolysis-stress test report generators automatically calculated the XF cell mito-stress and XF glycolysis stress test parameters from Wave data that have been exported to Excel, and all data were normalized to the total cell count per well using Celigo S image cytometry (Nexcelom Biosciences). Respiration and acidification rates are presented as the mean ± SD of three independent experiments in all experiments performed with 3 to 6 replicate wells in the Seahorse XFe96 analyzers.

Mitochondrial membrane potential measurement

After 24 h, 6DT1 cells treated with H_2O_2 were gently washed three times with 1× PBS buffer and then incubated in phenolred–free growth medium containing 50 nM of TMRM (Cat# 134361, Invitrogen) for 30 min in dark at 37 °C with 5% CO_2. After staining with the dye, stained cells were washed with 1× PBS and then incubated for 5 min at room temperature with 1:5000 DAPI to stain the nucleus. Then, the cells were prepared for imaging using Zeiss confocal microscopy at 100× oil-immersion objective.

Also, 6DT1 cells were grown in 24-well clear bottom plates (Cat# 353047, Falcon) and exposed to 1 μM H_2O_2 or 50 μM NAC or with both for 24 h. Then, media was gently removed from cells and replaced by 500 μl of 50 nM TMRM in phenol red–free DMEM complete growth medium and incubated at 37 °C for 20 min in dark. Cells were then washed three times with warmed 1× PBS, and fluorescence was measured using the TECAN infinite M200 plate reader with an excitation of 549 nm and emission of 575 nm.

Immunohistochemistry

Slides with formalin-fixed and paraffin-embedded sections of WT or CLIC4-KO 6DT1 murine mammary tumors excised from mammary fat pad of FVB mice after 28 days *in vivo* were subjected to immunohistochemistry using Leica Biosystems' BondRX auto-stainer with the following conditions: Epitope Retrieval 1 (Citrate), Caspase 3 antibody (Cat# 9661, Cell Signaling Technologies) at a dilution of 1:100, and the Bond Polymer Refine Detection Kit (Cat# DS9800, Leica Biosystems) with omission of the post-primary reagent. Isotype control antibody reagent was used in place of the Caspase3 antibody for the negative control.

Statistics

Graphs and statistical analyses were performed using Prism software (GraphPad Software Inc), and analysis of differences between two normally distributed test groups was performed using the student's *t* test. *p* values were considered statistically significant if $p < 0.05$.

Data availability

RNA-seq data is available in NCBI GEO database with the accession number GSE173997 and GSE188780.

Supporting information—This article contains supporting information.

Acknowledgments—This work was supported by the intramural program of the National Cancer Institute.
The authors would like to thank Kunio Nagashima and Christina Burks from Leidos Biomedical Research, Inc. Electron Microscopy Laboratory for generating the EM imaging for our cells and providing us with the detailed protocol. Also, thanks to Dr Richard Youle and Dr Susan Cheng from NINDS for their advice in quantifying the mitochondria from EM images. Thanks to Donna Butcher from Molecular Histopathology Laboratory for performing the immunohistochemistry staining of tumors. Thanks to Steve Jay and Susan Walters for taking care of the mouse colonies. This work was conducted through the support of the National Cancer Institute, Center for Cancer Research under Project Number ZIA BC 005445.

Author contributions—H. A. conceptulization and designing project; H. A., V. C. S., H. Y., and C. C. methodology; H. A., A. M. M., H. H. Y., and M. P. L. formal analysis; H. A. and S. H. Y. writing–original draft; L. L. and J. H. editing draft; S. H. Y. supervision and administration.

Conflict of interest—Authors declare that there are no competing interests.

Abbreviations—The abbreviations used are: CLIC4, chloride intracellular channel-4; EM, electron microscopy; FACS, fluorescence-activated cell sorting; GO, gene ontology; GSEA, gene set enrichment analysis; NAC, N-acetyl cysteine; OCR, oxygen consumption rate; PCA, principal component analysis; ROS, reactive oxygen species; SOD, superoxide dismutase; TMRM, tetramethylrhodamine, methyl ester.

References

1. Leone, A., Roca, M. S., Ciardiello, C., Costantini, S., and Budillon, A. (2017) Oxidative stress gene expression profile correlates with cancer patient poor prognosis: identification of crucial pathways might select novel therapeutic approaches. *Oxid. Med. Cell Longev.* **2017**, 2597581
2. Burdon, R. H. (1995) Superoxide and hydrogen peroxide in relation to mammalian cell proliferation. *Free Radic. Biol. Med.* **18**, 775–794
3. Hole, P. S., Pearn, L., Tonks, A. J., James, P. E., Burnett, A. K., Darley, R. L., *et al.* (2010) Ras-induced reactive oxygen species promote growth factor-independent proliferation in human CD34+ hematopoietic progenitor cells. *Blood* **115**, 1238–1246
4. Szatrowski, T. P., and Nathan, C. F. (1991) Production of large amounts of hydrogen peroxide by human tumor cells. *Cancer Res.* **51**, 794–798
5. Liou, G. Y., and Storz, P. (2010) Reactive oxygen species in cancer. *Free Radic. Res.* **44**, 479–496
6. Chiarugi, P., and Fiaschi, T. (2007) Redox signalling in anchorage-dependent cell growth. *Cell Signal.* **19**, 672–682
7. Rhee, S. G., Bae, Y. S., Lee, S. R., and Kwon, J. (2000) Hydrogen peroxide: a key messenger that modulates protein phosphorylation through cysteine oxidation. *Sci. STKE* **2000**, pe1
8. Storz, P. (2005) Reactive oxygen species in tumor progression. *Front. Biosci.* **10**, 1881–1896
9. Burdon, R. H., Gill, V., and Rice-Evans, C. (1990) Oxidative stress and tumour cell proliferation. *Free Radic. Res. Commun.* **11**, 65–76
10. Alexandrova, A. Y., Kopnin, P. B., Vasiliev, J. M., and Kopnin, B. P. (2006) ROS up-regulation mediates Ras-induced changes of cell morphology and motility. *Exp. Cell Res.* **312**, 2066–2073
11. Havre, P. A., O'Reilly, S., McCormick, J. J., and Brash, D. E. (2002) Transformed and tumor-derived human cells exhibit preferential sensitivity to the thiol antioxidants, N-acetyl cysteine and penicillamine. *Cancer Res.* **62**, 1443–1449
12. Martin, K. R., Saulnier, M. J., Kari, F. W., Barrett, J. C., and French, J. E. (2002) Timing of supplementation with the antioxidant N-acetyl-L-cysteine reduces tumor multiplicity in novel, cancer-prone p53 haploinsufficient Tg.AC (v-Ha-ras) transgenic mice but has no impact on malignant progression. *Nutr. Cancer* **43**, 59–66
13. Menon, S. G., Coleman, M. C., Walsh, S. A., Spitz, D. R., and Goswami, P. C. (2005) Differential susceptibility of nonmalignant human breast epithelial cells and breast cancer cells to thiol antioxidant-induced G(1)-delay. *Antioxid. Redox Signal.* **7**, 711–718
14. Lewis, A., Du, J., Liu, J., Ritchie, J. M., Oberley, L. W., and Cullen, J. J. (2005) Metastatic progression of pancreatic cancer: changes in antioxidant enzymes and cell growth. *Clin. Exp. Metastasis* **22**, 523–532
15. Kim, J., Kim, J., and Bae, J. S. (2016) ROS homeostasis and metabolism: a critical liaison for cancer therapy. *Exp. Mol. Med.* **48**, e269
16. Panieri, E., and Santoro, M. M. (2016) ROS homeostasis and metabolism: a dangerous liason in cancer cells. *Cell Death Dis.* **7**, e2253
17. Gorrini, C., Harris, I. S., and Mak, T. W. (2013) Modulation of oxidative stress as an anticancer strategy. *Nat. Rev. Drug Discov.* **12**, 931–947
18. Trachootham, D., Alexandre, J., and Huang, P. (2009) Targeting cancer cells by ROS-mediated mechanisms: a radical therapeutic approach? *Nat. Rev. Drug Discov.* **8**, 579–591
19. Chuang, J. Z., Milner, T. A., Zhu, M., and Sung, C. H. (1999) A 29 kDa intracellular chloride channel p64H1 is associated with large dense-core vesicles in rat hippocampal neurons. *J. Neurosci.* **19**, 2919–2928
20. Suh, K. S., Mutoh, M., Nagashima, K., Fernandez-Salas, E., Edwards, L. E., Hayes, D. D., *et al.* (2004) The organellular chloride channel protein CLIC4/mtCLIC translocates to the nucleus in response to cellular stress and accelerates apoptosis. *J. Biol. Chem.* **279**, 4632–4641
21. Littler, D. R., Harrop, S. J., Goodchild, S. C., Phang, J. M., Mynott, A. V., Jiang, L., *et al.* (2010) The enigma of the CLIC proteins: ion channels, redox proteins, enzymes, scaffolding proteins? *FEBS Lett.* **584**, 2093–2101
22. Singh, H., and Ashley, R. H. (2007) CLIC4 (p64H1) and its putative transmembrane domain form poorly selective, redox-regulated ion channels. *Mol. Membr. Biol.* **24**, 41–52
23. Al Khamici, H., Brown, L. J., Hossain, K. R., Hudson, A. L., Sinclair-Burton, A. A., Ng, J. P., *et al.* (2015) Members of the chloride intracellular ion channel protein family demonstrate glutaredoxin-like enzymatic activity. *PLoS One* **10**, e115699
24. Bohman, S., Matsumoto, T., Suh, K., Dimberg, A., Jakobsson, L., Yuspa, S., *et al.* (2005) Proteomic analysis of vascular endothelial growth factor-induced endothelial cell differentiation reveals a role for chloride intracellular channel 4 (CLIC4) in tubular morphogenesis. *J. Biol. Chem.* **280**, 42397–42404
25. Tung, J. J., Hobert, O., Berryman, M., and Kitajewski, J. (2009) Chloride intracellular channel 4 is involved in endothelial proliferation and morphogenesis *in vitro*. *Angiogenesis* **12**, 209–220
26. Ulmasov, B., Bruno, J., Gordon, N., Hartnett, M. E., and Edwards, J. C. (2009) Chloride intracellular channel protein-4 functions in angiogenesis by supporting acidification of vacuoles along the intracellular tubulogenic pathway. *Am. J. Pathol.* **174**, 1084–1096
27. Domingo-Fernandez, R., Coll, R. C., Kearney, J., Breit, S., and O'Neill, L. A. J. (2017) The intracellular chloride channel proteins CLIC1 and CLIC4 induce IL-1beta transcription and activate the NLRP3 inflammasome. *J. Biol. Chem.* **292**, 12077–12087
28. He, G., Ma, Y., Chou, S. Y., Li, H., Yang, C., Chuang, J. Z., *et al.* (2011) Role of CLIC4 in the host innate responses to bacterial lipopolysaccharide. *Eur. J. Immunol.* **41**, 1221–1230
29. Malik, M., Jividen, K., Padmakumar, V. C., Cataisson, C., Li, L., Lee, J., *et al.* (2012) Inducible NOS-induced chloride intracellular channel 4 (CLIC4) nuclear translocation regulates macrophage deactivation. *Proc. Natl. Acad. Sci. U. S. A.* **109**, 6130–6135
30. Raedler, D., Ballenberger, N., Klucker, E., Bock, A., Otto, R., Prazeres da Costa, O., *et al.* (2015) Identification of novel immune phenotypes for allergic and nonallergic childhood asthma. *J. Allergy Clin. Immunol.* **135**, 81–91
31. Suh, K. S., Mutoh, M., Mutoh, T., Li, L., Ryscavage, A., Crutchley, J. M., *et al.* (2007) CLIC4 mediates and is required for Ca2+-induced keratinocyte differentiation. *J. Cell Sci.* **120**, 2631–2640
32. Ronnov-Jessen, L., Villadsen, R., Edwards, J. C., and Petersen, O. W. (2002) Differential expression of a chloride intracellular channel gene, CLIC4, in transforming growth factor-beta1-mediated conversion of fibroblasts to myofibroblasts. *Am. J. Pathol.* **161**, 471–480
33. Yao, Q., Qu, X., Yang, Q., Wei, M., and Kong, B. (2009) CLIC4 mediates TGF-beta1-induced fibroblast-to-myofibroblast transdifferentiation in ovarian cancer. *Oncol. Rep.* **22**, 541–548
34. Shukla, A., Edwards, R., Yang, Y., Hahn, A., Folkers, K., Ding, J., *et al.* (2014) CLIC4 regulates TGF-beta-dependent myofibroblast differentiation to produce a cancer stroma. *Oncogene* **33**, 842–850
35. Suh, K. S., Mutoh, M., Gerdes, M., Crutchley, J. M., Mutoh, T., Edwards, L. E., *et al.* (2005) Antisense suppression of the chloride intracellular channel family induces apoptosis, enhances tumor necrosis factor {alpha}-induced apoptosis, and inhibits tumor growth. *Cancer Res.* **65**, 562–571
36. Suh, K. S., Crutchley, J. M., Koochek, A., Ryscavage, A., Bhat, K., Tanaka, T., *et al.* (2007) Reciprocal modifications of CLIC4 in tumor epithelium and stroma mark malignant progression of multiple human cancers. *Clin. Cancer Res.* **13**, 121–131
37. Suh, K. S., Malik, M., Shukla, A., Ryscavage, A., Wright, L., Jividen, K., *et al.* (2012) CLIC4 is a tumor suppressor for cutaneous squamous cell cancer. *Carcinogenesis* **33**, 986–995
38. Tang, H. Y., Beer, L. A., Tanyi, J. L., Zhang, R., Liu, Q., and Speicher, D. W. (2013) Protein isoform-specific validation defines multiple chloride intracellular channel and tropomyosin isoforms as serological biomarkers of ovarian cancer. *J. Proteomics* **89**, 165–178
39. Okudela, K., Katayama, A., Woo, T., Mitsui, H., Suzuki, T., Tateishi, Y., *et al.* (2014) Proteome analysis for downstream targets of oncogenic KRAS–the potential participation of CLIC4 in carcinogenesis in the lung. *PLoS One* **9**, e87193
40. Zou, Q., Yang, Z., Li, D., Liu, Z., and Yuan, Y. (2016) Association of chloride intracellular channel 4 and Indian hedgehog proteins with survival of patients with pancreatic ductal adenocarcinoma. *Int. J. Exp. Pathol.* **97**, 422–429
41. Singha, B., Harper, S. L., Goldman, A. R., Bitler, B. G., Aird, K. M., Borowsky, M. E., *et al.* (2018) CLIC1 and CLIC4 complement CA125 as a

diagnostic biomarker panel for all subtypes of epithelial ovarian cancer. *Sci. Rep.* **8**, 14725
42. Faraji, F., Pang, Y. L., Walker, R. C., Borges, R. N., Yang, L., and Hunter, K. W. (2012) Cadm1 is a metastasis susceptibility gene that suppresses metastasis by modifying tumor interaction with the cell-mediated immunity. *PLoS Genet.* **8**, e1002926
43. Nagashima, K., Zheng, J. W., Parmiter, D., and Patri, A. K. (2011) Biological tissue and cell culture specimen preparation for TEM nanoparticle characterization. *Methods Mol. Biol.* **697**, 83–91
44. Weydert, C. J., Waugh, T. A., Ritchie, J. M., Iyer, K. S., Smith, J. L., Li, L., *et al.* (2006) Overexpression of manganese or copper-zinc superoxide dismutase inhibits breast cancer growth. *Free Radic. Biol. Med.* **41**, 226–237
45. Hecht, F., Pessoa, C. F., Gentile, L. B., Rosenthal, D., Carvalho, D. P., and Fortunato, R. S. (2016) The role of oxidative stress on breast cancer development and therapy. *Tumour Biol.* **37**, 4281–4291
46. Gururaja Rao, S., Patel, N. J., and Singh, H. (2020) Intracellular chloride channels: novel biomarkers in diseases. *Front. Physiol.* **11**, 96
47. Yang, Y., Yang, H. H., Hu, Y., Watson, P. H., Liu, H., Geiger, T. R., *et al.* (2017) Immunocompetent mouse allograft models for development of therapies to target breast cancer metastasis. *Oncotarget* **8**, 30621–30643
48. Fridovich, I. (1997) Superoxide anion radical (O2-.), superoxide dismutases, and related matters. *J. Biol. Chem.* **272**, 18515–18517
49. Ponnalagu, D., Rao, S. G., Farber, J., Xin, W. Y., Hussain, A. T., Shah, K., *et al.* (2016) Molecular identity of cardiac mitochondrial chloride intracellular channel proteins. *Mitochondrion* **27**, 6–14
50. Fernandez-Salas, E., Suh, K. S., Speransky, V. V., Bowers, W. L., Levy, J. M., Adams, T., *et al.* (2002) mtCLIC/CLIC4, an organellular chloride channel protein, is increased by DNA damage and participates in the apoptotic response to p53. *Mol. Cell. Biol.* **22**, 3610–3620
51. Pierelli, G., Stanzione, R., Forte, M., Migliarino, S., Perelli, M., Volpe, M., *et al.* (2017) Uncoupling protein 2: a key player and a potential therapeutic target in vascular diseases. *Oxid. Med. Cell Longev.* **2017**, 7348372
52. Haynes, C. M., Titus, E. A., and Cooper, A. A. (2004) Degradation of misfolded proteins prevents ER-derived oxidative stress and cell death. *Mol. Cell* **15**, 767–776
53. Redza-Dutordoir, M., and Averill-Bates, D. A. (2016) Activation of apoptosis signalling pathways by reactive oxygen species. *Biochim. Biophys. Acta Mol. Cell Res.* **1863**, 2977–2992
54. Yang, H., Villani, R. M., Wang, H., Simpson, M. J., Roberts, M. S., Tang, M., *et al.* (2018) The role of cellular reactive oxygen species in cancer chemotherapy. *J. Exp. Clin. Cancer Res.* **37**, 266
55. Chocry, M., Leloup, L., and Kovacic, H. (2017) Reversion of resistance to oxaliplatin by inhibition of p38 MAPK in colorectal cancer cell lines: involvement of the calpain/Nox1 pathway. *Oncotarget* **8**, 103710–103730
56. Alexandre, J., Hu, Y., Lu, W., Pelicano, H., and Huang, P. (2007) Novel action of paclitaxel against cancer cells: bystander effect mediated by reactive oxygen species. *Cancer Res.* **67**, 3512–3517
57. Egawa, N., Tanaka, T., Matsufuji, S., Yamada, K., Ito, K., Kitagawa, H., *et al.* (2021) Antitumor effects of low-dose tipifarnib on the mTOR signaling pathway and reactive oxygen species production in HIF-1alpha-expressing gastric cancer cells. *FEBS Open Bio* **11**, 1465–1475
58. Jiao, D., Cai, Z., Choksi, S., Ma, D., Choe, M., Kwon, H. J., *et al.* (2018) Necroptosis of tumor cells leads to tumor necrosis and promotes tumor metastasis. *Cell Res.* **28**, 868–870
59. Xu, Y., Kang, J., Yuan, Z., Li, H., Su, J., Li, Y., *et al.* (2013) Suppression of CLIC4/mtCLIC enhances hydrogen peroxide-induced apoptosis in C6 glioma cells. *Oncol. Rep.* **29**, 1483–1491
60. Xue, H., Lu, J., Yuan, R., Liu, J., Liu, Y., Wu, K., *et al.* (2016) Knockdown of CLIC4 enhances ATP-induced HN4 cell apoptosis through mitochondrial and endoplasmic reticulum pathways. *Cell Biosci.* **6**, 5
61. Zhong, J., Kong, X., Zhang, H., Yu, C., Xu, Y., Kang, J., *et al.* (2012) Inhibition of CLIC4 enhances autophagy and triggers mitochondrial and ER stress-induced apoptosis in human glioma U251 cells under starvation. *PLoS One* **7**, e39378
62. Liu, L., Zhou, X., Shetty, S., Hou, G., Wang, Q., and Fu, J. (2019) HDAC6 inhibition blocks inflammatory signaling and caspase-1 activation in LPS-induced acute lung injury. *Toxicol. Appl. Pharmacol.* **370**, 178–183
63. Zhang, Y. X., Ying, Y. Y., Zhou, L., Fu, J. J., Shen, Y. P., and Ke, C. F. (2019) Exposure to Chinese famine in early life modifies the association between hyperglycaemia and cardiovascular disease. *Nutr. Metab. Cardiovasc. Dis.* **29**, 1230–1236
64. Patel, D., Ythier, D., Brozzi, F., Eizirik, D. L., and Thorens, B. (2015) Clic4, a novel protein that sensitizes beta-cells to apoptosisa. *Mol. Metab.* **4**, 253–264
65. Arnould, T., Mercy, L., Houbion, A., Vankoningsloo, S., Renard, P., Pascal, T., *et al.* (2003) MtCLIC is up-regulated and maintains a mitochondrial membrane potential in mtDNA-depleted L929 cells. *FASEB J.* **17**, 2145
66. Palmfeldt, J., Vang, S., Stenbroen, V., Pavlou, E., Baycheva, M., Buchal, G., *et al.* (2011) Proteomics reveals that redox regulation is disrupted in patients with ethylmalonic encephalopathy. *J. Proteome Res.* **10**, 2389–2396
67. Feng, Z. L., Zhu, Z. B., Chen, W., Bai, Y., Hu, D. H., and Cheng, J. (2020) Chloride intracellular channel 4 participate in the protective effect of Ginkgolide B in MPP plus injured MN9D cells: insight from proteomic analysis. *Clin. Proteomics* **17**, 32
68. Argenzio, E., and Moolenaar, W. H. (2016) Emerging biological roles of Cl- intracellular channel proteins. *J. Cell Sci.* **129**, 4165–4174
69. Gururaja Rao, S., Ponnalagu, D., Patel, N. J., and Singh, H. (2018) Three decades of chloride intracellular channel proteins: from organelle to organ physiology. *Curr. Protoc. Pharmacol.* **80**, 11.21.1–11.21.17
70. Shpilka, T., and Haynes, C. M. (2018) The mitochondrial UPR: mechanisms, physiological functions and implications in ageing. *Nat. Rev. Mol. Cell Biol.* **19**, 109–120
71. Melber, A., and Haynes, C. M. (2018) UPR(mt) regulation and output: a stress response mediated by mitochondrial-nuclear communication. *Cell Res.* **28**, 281–295
72. Pai, H. V., Starke, D. W., Lesnefsky, E. J., Hoppel, C. L., and Mieyal, J. J. (2007) What is the functional significance of the unique location of glutaredoxin 1 (GRx1) in the intermembrane space of mitochondria? *Antioxid. Redox Signal.* **9**, 2027–2033
73. Hernandez-Fernaud, J. R., Ruengeler, E., Casazza, A., Neilson, L. J., Pulleine, E., Santi, A., *et al.* (2017) Secreted CLIC3 drives cancer progression through its glutathione-dependent oxidoreductase activity. *Nat. Commun.* **8**, 14206
74. Faraji, F., Pang, Y., Walker, R. C., Nieves Borges, R., Yang, L., and Hunter, K. W. (2012) Cadm1 is a metastasis susceptibility gene that suppresses metastasis by modifying tumor interaction with the cell-mediated immunity. *PLoS Genet.* **8**, e1002926
75. Dobin, A., Davis, C. A., Schlesinger, F., Drenkow, J., Zaleski, C., Jha, S., *et al.* (2013) STAR: ultrafast universal RNA-seq aligner. *Bioinformatics* **29**, 15–21
76. Li, B., and Dewey, C. N. (2011) RSEM: accurate transcript quantification from RNA-seq data with or without a reference genome. *BMC Bioinformatics* **12**, 323
77. Love, M. I., Huber, W., and Anders, S. (2014) Moderated estimation of fold change and dispersion for RNA-seq data with DESeq2. *Genome Biol.* **15**, 550
78. Perez-Guijarro, E., Yang, H. H., Araya, R. E., El Meskini, R., Michael, H. T., Vodnala, S. K., *et al.* (2020) Multimodel preclinical platform predicts clinical response of melanoma to immunotherapy. *Nat. Med.* **26**, 781–791
79. Subramanian, A., Tamayo, P., Mootha, V. K., Mukherjee, S., Ebert, B. L., Gillette, M. A., *et al.* (2005) Gene set enrichment analysis: a knowledge-based approach for interpreting genome-wide expression profiles. *Proc. Natl. Acad. Sci. U. S. A.* **102**, 15545–15550
80. Chen, H., and Boutros, P. C. (2011) VennDiagram: a package for the generation of highly-customizable Venn and Euler diagrams in R. *BMC Bioinformatics* **12**, 35
81. Huang, D. W., Sherman, B. T., and Lempicki, R. A. (2009) Systematic and integrative analysis of large gene lists using DAVID bioinformatics resources. *Nat. Protoc.* **4**, 44–57
82. Walter, W., Sanchez-Cabo, F., and Ricote, M. (2015) GOplot: an R package for visually combining expression data with functional analysis. *Bioinformatics* **31**, 2912–2914
83. Cataisson, C., Salcedo, R., Michalowski, A. M., Klosterman, M., Naik, S., Li, L., *et al.* (2019) T-cell deletion of MyD88 connects IL17 and IkappaBzeta to RAS oncogenesis. *Mol. Cancer Res.* **17**, 1759–1773